NREL/TP-451-7162 • UC Category: 1263 • DE94011886

Thin-Film Cadmium Telluride Photovoltaic Cells

Final Subcontract Report 1 November 1992 – 1 January 1994

A. D. Compaan, R. G. Bohn
University of Toledo
Toledo, Ohio

NREL technical monitor: B. von Roedern

National Renewable Energy Laboratory
1617 Cole Boulevard
Golden, Colorado 80401-3393
A national laboratory of the U.S. Department of Energy
Managed by Midwest Research Institute
for the U.S. Department of Energy
under contract No. DE-AC36-83CH10093

Prepared under Subcontract No. ZN-1-19019-3

September 1994

NOTICE

Available to DOE and DOE contractors from:
Office of Scientific and Technical Information (OSTI)
P.O. Box 62
Oak Ridge, TN 37831
Prices available by calling (615) 576-8401

Available to the public from:
National Technical Information Service (NTIS)
U.S. Department of Commerce
5285 Port Royal Road
Springfield, VA 22161
(703) 487-4650


Printed on paper containing at least 50% wastepaper and 10% postconsumer waste

SUMMARY

The major emphasis of this program at the University of Toledo (UT) is the development and optimization of radio-frequency sputtering for the deposition of thin films of cadmium telluride (CdTe) and related semiconductors for thin-film solar cells. Pulsed laser physical vapor deposition (LPVD) is also used at UT for exploratory work on these materials especially where alloying or doping are involved and for the deposition of cadmium chloride layers. The sputtering work has utilized a two-inch diameter planar magnetron sputter gun. The film growth rate by rf sputtering has been studied as a function of substrate temperature, gas pressure, and rf power. For a wide range of growth conditions, we have determined film stoichiometry, crystallographic orientation, and grain size, as well as electrical and optical properties of the films. Characterization measurements performed at UT include x-ray diffraction, SEM/EDS, photoluminescence, Raman, double-beam optical absorption, photoreflectance and electroreflectance, Hall effect, electrical conductivity, current-voltage (I-V), spectral quantum efficiency (SQE), and optical-beam-induced-current (OBIC) measurements.

Complete solar cells have been fabricated starting from tin-oxide-coated soda-lime glass substrates. We are able regularly to fabricate an array of cells on three-inch square substrates with good uniformity and reproducibility. Open circuit voltages regularly exceed 0.81 V and have reached 0.84 V with fill factors up to 72%. During the year, some studies also were made on rf sputtering of ZnTe doped with Cu and reactive sputtering of ZnTe doped with N for use as a contact layer to the CdTe. Current efforts are addressing improvements in the open circuit voltage by variations to the CdTe-based absorber layer and in the short circuit current by modifications to the CdS window layer.

Table of Contents

LIST OF FIGURES

1.0 Introduction

1.1 Background

This final report covers research which began in July of 1990 as a joint project involving the University of Toledo, Solar Cells Inc (SCI), and Glasstech Solar Inc (GSI). GSI has since ceased operations and terminated its participation. On the other hand, SCI has moved rapidly toward module production and therefore a separate contract was negotiated between SCI and NREL. SCI remained as a lower-tier subcontractor with UT only through the end of the first contract year. Accordingly, the contract with UT was renegotiated to reflect these changes and the University of Toledo picked up some of the work initially planned for GSI--principally the effort on rf sputtering. The University of Toledo work no longer includes major efforts on scale-up to commercialization, but retains the emphasis on basic science and the further development of the laser deposition and rf sputtering processes. Although official participation of SCI in this project has ceased, we have maintained considerable communication and frequent collaboration with SCI. This involved the occasional exchange of thin films, cooperation in the use of facilities including at SCI a stylus profilometer and a calibrated solar standard. Students or faculty at UT have assisted SCI with occasional film growth by sputtering, double-beam optical absorption measurements, Raman and photoluminescence measurements, and Hall measurements.

The first year of effort yielded promising results for complete cells fabricated by the pulsed laser physical vapor deposition (LPVD) method. Also the first rf sputtered CdTe films were grown at the end of the year. During the second year, the UT group placed increasing emphasis on optimization of the rf sputtering method for deposition of CdTe and, late in the year CdS films were also deposited so that the first all-sputtered cells could be produced. One of these sputtered cells was tested by NREL at 10.4% and simultaneously an all-LPVD cell was tested at 10.5%.

In the third year of NREL support, considerable effort was placed on understanding the important parameters controlling the sputtered film deposition rate and film quality. The laser-driven physical vapor deposition (LPVD) system was modified to obtain more uniform deposition and the substrate heater system redesigned to permit work in oxygen ambients. The LPVD system continues to be used for the dry application of $CdCl_2$ layers. In device fabrication, we regularly achieve uniform and reproducible devices over a ~3 inch square substrate with AM1.5 efficiencies above 10% and $V_{oc} > 0.8$ V. The highest V_{oc} tested in our laboratory was just over 0.84 V. Fill factors up to 72.3% have been obtained. During the year, we have instrumented and tested a system for photoreflectance and electroreflectance which shows considerable potential for studying the properties of the CdTe interfaces with CdS, air and Cu/Au.

1.2 Technical Approach (three-year overview)

Laser deposition--The photovoltaics effort of the UT group began with study of the laser-driven physical vapor deposition process (LPVD) for CdS/CdTe cell fabrication. The LPVD process combines the advantages of (ultra)high vacuum cleanliness and monolayer control over the growth interface. It has many similarities to molecular beam epitaxy. This growth process was studied intensively during the first contract year (Phase One) during which complete CdS/CdTe solar cells were fabricated with NREL-tested efficiencies up to 8.7%.[1,2] During Phase Two a

variety of adjustments were made to the LPVD process and to the post-deposition processing which yielded an NREL-tested efficiency of 10.5%.[3-10] During Phase Three the laser deposition system was modified to accept standard two-inch diameter sputter targets. The system can now be loaded with up to four targets simultaneously (e.g., CdS, CdTe, ZnTe and $CdCl_2$). In addition, the substrate heater was modified to use two linear tungsten-halogen lamps and is capable of operation in air or O_2 at temperatures up to 500 °C. The use of commercial, sintered, two-inch sputter targets has so far yielded no improvement in cell efficiency although the deposited layers have much greater spatial uniformity due to the scanned laser beam, rotation of the target and rotation of the substrate. Although the LPVD technique has permitted convenient control over target fabrication, since small cold-pressed targets could be used, the method appears difficult to scale up for economical deposition of square-meter film areas.

During Phase Three LPVD remained our method of choice for the deposition of the $CdCl_2$-layer in both sputtered and LPVD solar cells. LPVD is also used regularly for preliminary studies of alloy materials, for doping studies, and for growth of CdTe in reactive ambients. A limited number of "all-LPVD" cells were fabricated with this system during the past year.

Rf sputtering--The first sputtered CdTe films were deposited at the end of the first phase. During Phase Two major effort was given to the optimization of the rf sputtering process through studies of as-deposited individual film quality and as well as cell fabrication and testing. During this year CdS was sputter-deposited for the first time. Completed cells were fabricated with sputtered CdTe and LPVD CdS; for the first time cells were fabricated also by using rf sputtering for both the CdS and CdTe layers. LPVD was still used for the deposition of a $CdCl_2$ layer prior to the usual 400°C air anneal. For both laser-deposited cells and the rf sputtered cells, LOF SnO_2-coated soda-lime glass (10Ω/square) continues to be used and our standard contact method has been a thin layer of copper followed by a gold cap.

During Phase Three we have made detailed studies of the dependence of the sputtered film growth rate on the substrate temperature, gas pressure, and rf power. The dependence of film characteristics (grain size, crystallographic orientation, electrical transport properties, and optical properties) on these growth parameters were also obtained. Additional efforts focussed on the growth of ZnTe with some attention given to doping with Cu and with N by reactive sputtering. Using the LPVD system, we have examined the effect of the presence of oxygen during film growth and its consequences on the CdS/CdTe interface properties. Finally, we have implemented a photoreflectance/electroreflectance (PR/ER) system which has proved quite useful for studies of CdTe interfaces.

Materials characterization/device testing--Much materials characterization continues to be used to help optimize the deposition conditions. This includes, in addition to the PR/ER system, optical absorption, scanning electron microscopy with energy dispersive x-ray spectroscopy (SEM/EDS), x-ray diffraction, Raman scattering, photoluminescence (PL), electrial conductivity and Hall measurements. During the year, the Raman and PL system was upgraded with a cooled CCD detector (1152 x 298) obtained with independent funds. These efforts were supplemented by additional measurements performed at NREL (carrier lifetime, electron beam induced current) and at Colorado State University (detailed solar cell loss analysis).

2.0 Advances in Film Deposition and Cell Fabrication

2.1 RF Sputtering of CdTe

During the past year the single gun rf sputtering system has been modified slightly with the addition of a manual shutter over the two-inch diameter planar magnetron sputter gun from AJA International. Also we have installed an MKS exhaust butterfly valve controlled via a capacitance manometer. Deposition is done under constant argon sputter gas pressure with the gas flow typically set at ~14 sccm. A sketch of the present system is given in Fig. 2-1. Deposition is upward with the substrates radiatively heated by a twenty-loop tantalum wire heater. The target-to-substrate distance is 7 cm. A brief attempt was made during the year to use two 2-inch guns side-by-side, one with CdS and one with CdTe. However, the results were poor and the effort was discontinued. The poor solar cell performance may arise from proximity effects of the adjacent magnetic fields of the sputtering guns (unlikely, we think), cross contamination, or incompatible grain morphology between the CdS and CdTe (sputtered from different directions).

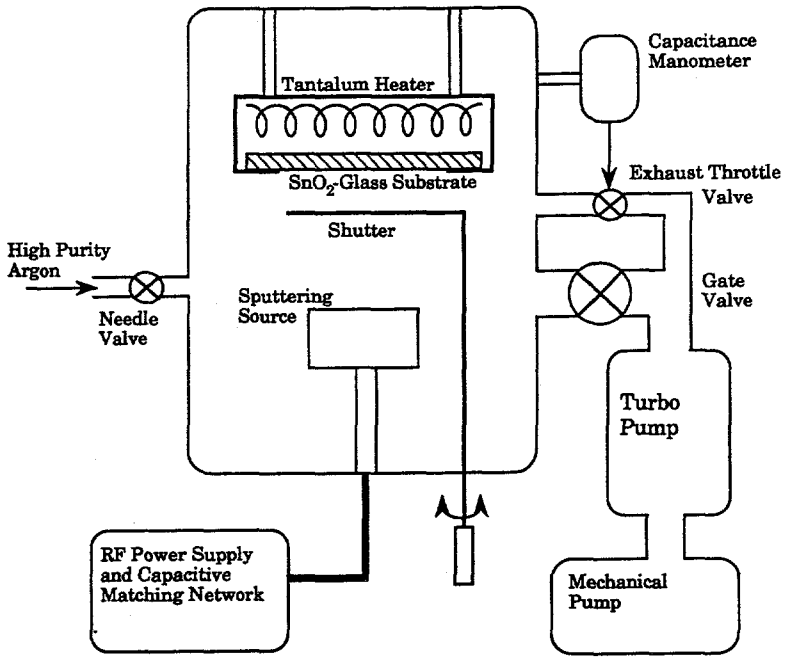

Fig. 2-1: RF sputter deposition system accomodating two-inch diameter targets and 3-inch square substrates.

This single gun system has been used for the growth of individual films of CdTe, CdS, ZnTe and ZnO on borosilicate glass and on uncoated and SnO_2-coated soda-lime glass. Most of the effort on individual film growth was focussed on the growth of CdTe and ZnTe. For CdTe, studies were conducted of the dependence of growth rate and film quality on substrate temperature, gas pressure, and rf power. Details are provided below in Sections 2.1.1 to 2.1.4. For ZnTe films, studies of doping with Cu were performed and doping by reactive sputtering with nitrogen were made. See Section 2.2 below.

If sputtering is to be used for large-area depositions, it is important to obtain the highest possible growth rates consistent with high film quality. It is also important to determine to what extent the growth rate and film quality depend on the depth of the target erosion track. Thus we have

studied the CdTe film growth rate for two conditions--deep target erosion and fresh (planar) target surface.

2.1.1 Target erosion effects

For large-area depositions, efficient sputter target utilization is important. Ideally, it should be possible to deposit high quality films from a fresh target as well as from a deeply eroded target. We tested the effect of target erosion by comparing the film quality obtained from an old, deeply eroded two-inch diameter target with the quality obtained from a fresh target. Both targets were hot-pressed discs two inches in diameter and 1/4 inch thick. The old, eroded target had a circular track almost 1/4 inch deep. In fact, at the end of the series of depositions, the erosion track finally punched completely through the target. A cross sectional profile of the erosion is shown in Fig. 2-2. This trace gives a clear indication of the region of most intense sputtering for the magnetic field configuration of the AJA planar magnetron sputtering gun. Measure-ments of target mass showed that ~30% of the target had been sputtered. SEM/EDS measurements of film stoichiometry as well as PL spectra of films sputtered from the old and new targets indicated no differences within the experimental error of about ±2%. In addition, both targets yielded cells with AM1.5 efficiencies above 10%. Therefore, we conclude that target erosion appears to have little effect on performance of the finished solar cells--at least at the present ~10% efficiency level.

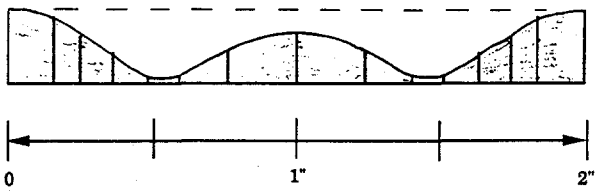

Fig. 2-2: Profile of deeply eroded CdTe target.

Although no effect of target erosion was observed on cell efficiencies, there was a substantial difference in the film growth rate for the old (deeply eroded) and new CdTe sputtering targets. The data of Figs. 2-3, 2-4, and 2-5 below show that the film growth rate is approximately a factor of two higher for the old, eroded target than for the fresh target with the planar surface. We believe that this effect may be related to the greater surface area of the old target although we cannot rule out some contribution from additional heating of the target in very thin regions which may have had poor thermal contact to the copper cooling block. In fact SEM studies of the old target showed evidence of melting at the bottom of the erosion track.

2.1.2 Substrate temperature dependence

For typical polycrystalline thin-film growth, the grain size increases as the substrate temperature rises. Larger grains are expected to be advantageous in polycrystalline photovoltaics since the total grain boundary surface area decreases with larger grains. However, as the substrate temperature rises the sticking coefficients fall and growth rates decrease. This behavior is shown in Fig. 2-3 for our typical gas pressure (18 mT) and flow rate (14 sccm) and for moderate rf power (120 W). The general trend for both eroded and fresh targets shows that the deposition rate falls rapidly in the range between 350 and 425°C. Presumably this trend is a result of reduced sticking coefficients for the Cd and Te atoms on the higher temperature substrate surface. CdTe films have been grown on SnO_2/glass as well as CdS/SnO_2/glass with no substantial difference in growth rate.

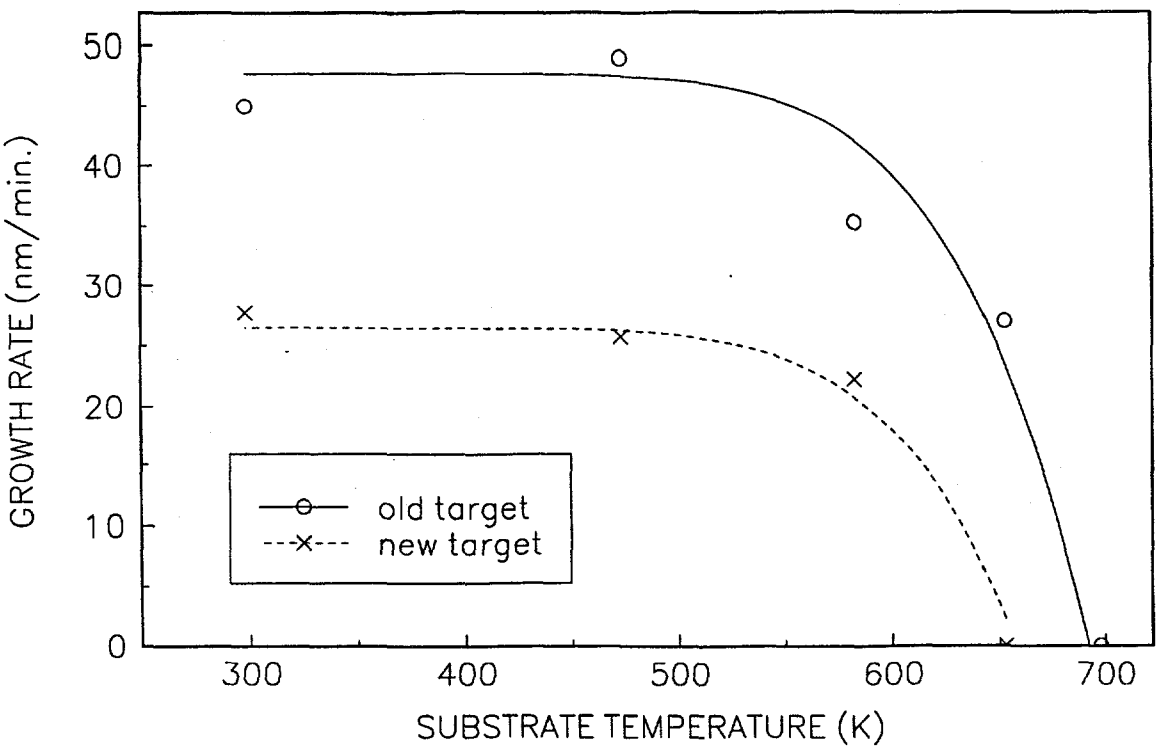

Fig. 2-3: *Growth rate of sputtered CdTe films vs. substrate temperature. Pressure = 18 mTorr;* P_{rf} *= 120 Watts.* o *- eroded target; x - fresh target. Curves according to Eq. 1.*

Note in Fig. 2-3 that the target condition (old, deeply eroded vs. fresh, planar) has a strong effect on the rf sputtering rate. The targets were 0.25 inch thick unbacked 2 inch diameter CdTe discs. The erosion track of the deeply eroded target was approximately 0.24 inch deep. See Fig. 2-2. We believe that the higher sputter rate for the eroded target is largely a result of the non-planar profile although the target temperature at the bottom of the track is likely to be increased due to the poor thermal conductivity of the CdTe and the boundary layer at the interface between the CdTe and the water-cooled copper head of the sputter gun. (Thermal contact was made only by the positive pressure of the clamping ring.) Fig. 2-3 shows that the eroded target produces film growth rates almost a factor of two higher than does the fresh target. SEM/EDS measurements across the two target surfaces show that there is very little change in *target* stoichiometry for the two extreme cases of target condition. Furthermore, the as-grown *films* also show no difference in stoichiometry within the measurement accuracy of ±2%.

The solid and dashed curves in Fig. 2-3 are fits of the growth rate data to the functional form appropriate for balance between incident flux A and reevaporation:[11]

$$\text{growth rate (nm/min)} = A - BT^2 \sinh(h\nu/2kT) \exp(-\Phi_a/kT), \qquad \text{Eq. (1)}$$

where A represents the incident flux from the sputtering gun and the second term, following Kubo,[11] represents the flux of atoms leaving the surface of the film. We find that A = 26 and

47 nm/min for the fresh and eroded targets respectively. B = 4600, $\nu = 4.8 \times 10^{12}$ Hz is the optic phonon frequency for CdTe, and $\Phi_a = 0.73$ eV for both data sets. The curves show that both sets of data (for the two target conditions) may be fit well by changing only the incident flux with the eroded target having a higher flux by a factor of ~1.8. Note that the evaporation flux (or non-sticking component of the incident flux) is likely to be controlled by the behavior of that binary component which has the higher vapor pressure, namely Cd.

2.1.3 rf power dependence

As the rf power increases in planar magnetron sputtering, the target or cathode develops an increasing DC self-bias potential relative to the anode ring and most other parts of the chamber including the substrate and the chamber walls. It is this negative self bias of the target which provides the acceleration energy for Ar^+ ions across the cathode sheath leading to sputtering from the target. We have measured the target self bias as a function of rf power taking care to maintain good impedance matching at each power level. Fig. 2-4 displays the target DC self-bias voltage as a function of the rf power, P, input into the capacitively coupled matching network. The DC self-bias voltage of the target follows the empirical relation

$$V_{DC} \sim A[(P/P_0)-1]^r, \qquad \text{Eq. (2)}$$

where $P_0 = 20$ W is the plasma ignition threshold power (roughly independent of pressure) and the constants A and r depend only weakly on pressure. The solid curve in Fig. 2-4 gives A = 70 V and r = 0.4. Note that the fit is almost independent of sputter gas pressure between 3 and 50 mTorr.

We are not aware of similar results in the literature for rf planar magnetron sputtering, but for DC planar magnetron sputtering, the commonly observed[12] current-voltage relation is $I = kV^n$. Since power is the product of the cathode potential and the current, this becomes $P = kV^{n+1}$. Inverting this expression, the DC magnetron observations indicate that

$$V \sim k'P^{1/(n+1)}. \qquad \text{Eq. (3)}$$

Thus our observed value of r=0.4 is equivalent to n = 1.5, for rf powers above threshold power P_0. This value of n is low compared with the range of values usually observed for DC magnetron sputtering ($3 < n < 15$).[12]

The film growth rate vs. rf power is shown in Fig. 2-5a for a substrate temperature of 310°C, again for the two target conditions. Note that the deposition rate increases monotonically with power but at a rate which is sublinear in rf power. (The power indicated here is the input power to the

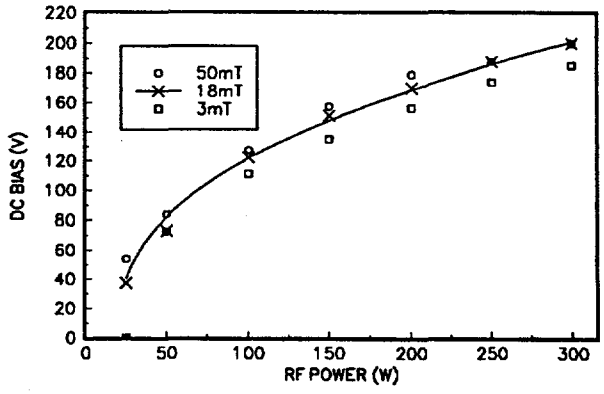

Fig. 2-4: Target self-bias voltage vs. input rf power.

matchbox. During the sputter deposition, the rf matching network is adjusted for a reflected power of less than 1 Watt and we estimate that about half of the incident power is dissipated in the planar magnetron gun with the balance dissipated in the inductance of the matching network. The threshold power for sustaining a discharge is about 20 W. In Fig. 2-5b we show the same data plotted as a function of the (DC) self-bias voltage. These data indicate that the growth rate is nearly linear in the self-bias voltage above a threshold of ~80 Volts DC.

Although there are no published studies, to our knowledge, of sputtering yields of Ar on CdTe, measurements of the sputtering yield of Ar ions incident on Cu at low energy (E < 500 eV) show a linear increase with ion energy above a threshold of ~25 eV.[12] Thus, our observed linear dependence on self-bias voltage is in qualitative agreement with this study of sputtering of Cu. From our measurements we conclude that the threshold energy for sputtering of CdTe by Ar^+ is ~80 eV. (See Fig. 2-5b.)

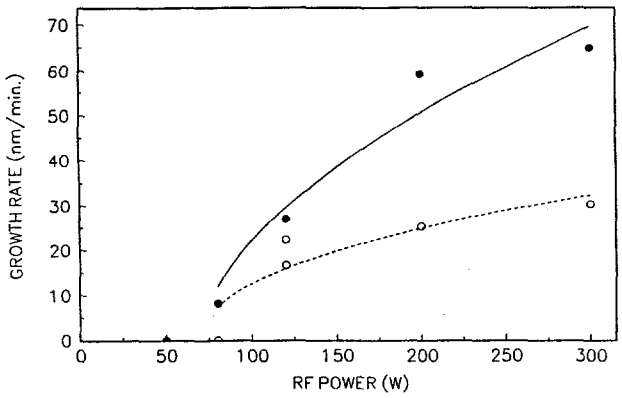

Fig. 2-5a: Growth rate of CdTe vs. rf power. T_s=310C; p=18 mTorr; •/○ = eroded/new target.

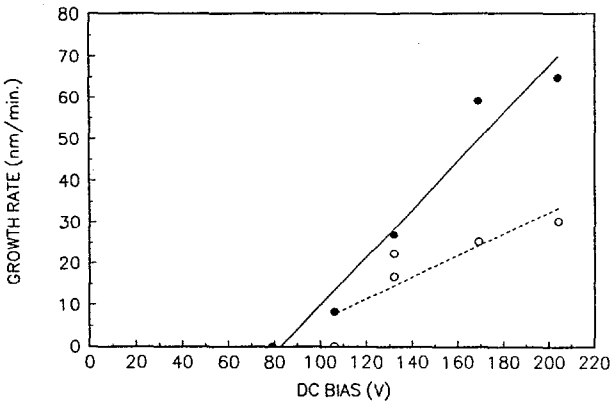

Fig. 2-5b: Growth rate of CdTe vs. self-bias voltage. T_s=310C; p=18mT.

2.1.4 Gas pressure dependence

As the gas pressure increases above 3 mTorr, the sputtered atoms incur increasing numbers of collisions between the target and substrate. As a consequence, kinetic energy will be lost from the sputtered species and additional atoms may be scattered out of the plume before reaching the substrate. Fig. 2-6 shows the effect of Ar pressure on the growth rate of CdTe films for a substrate temperature of 310 °C and rf power of 120 W. For reference, the mean free path, λ, of a neutral Cd atom in a neutral background of Ar, as estimated from kinetic theory calculations ($\lambda = k_B T/\pi d^2 P 2^{1/2}$, where d is a scattering diameter and P is the pressure), is ~6 mm at 10 mTorr and 300K. The growth rate data show little dependence on the gas pressure even up to 50 mTorr where the ratio of target-substrate distance to mean free path is 35. Apparently diffusion out of the plume does not play a major role in the fluence impacting the substrate. The reduced kinetic energy of atoms impacting the growth surface may also increase the sticking coefficient and thus tend to compensate for scattering out of the plume. Below 3 mTorr the growth rate decreases rapidly presumably due to reduced plasma density.

Changes in substrate temperature, rf power, and gas pressure also affect the characteristics of the as-grown films. These effects are described in Section 3 below.

2.2 RF Sputtering of ZnTe

The rf sputtering characteristics of ZnTe are very similar to CdTe except that ZnTe can be sputtered at slightly higher substrate temperatures--up to ~470 °C. We performed some limited studies of the growth rate dependence on substrate temperature and gas pressure. The results are summarized in Table 2.1. (Note that these films were grown with a 5% N_2 addition to the Ar sputter gas. However, the growth rate is not substantially affected by the additional N_2.) In comparison with the results for CdTe, the dependence on rf power (seen by comparing samples ZT77, ZT80, and ZT81) is similar with a growth rate about 75% of that for CdTe. The ZnTe will tolerate slightly higher substrate temperatures (see the series of samples ZT76-ZT79) before the sticking coefficients become negligible. We have successfully grown films up to T_s=470°C.

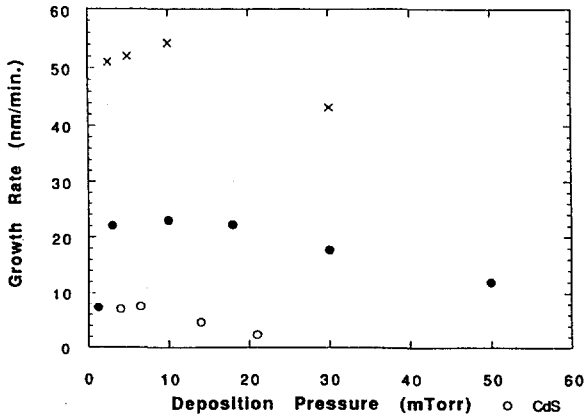

Fig. 2-6: Growth rate vs. Ar gas pressure. (T_s=310 C; P_{rf} = 120 W; x/• = eroded/fresh CdTe target; O = CdS.)

TABLE 2.1: Sputtered ZnTe growth rate dependence on T_s and P_{rf}

SAMPLE ID	T_s (°C)	p (mTorr) [5% N_2/(Ar+N_2)]	P_{rf}(W)	growth rate (nm/min)	$\sigma(\Omega\text{-cm})^{-1}$
ZT76	400	12	150	9	7E-3
ZT77	370	12	150	14	8E-3
ZT78	430	12	150	8	5E-3
ZT79	335	12	150	18	4E-3
Z780	370	12	200	17	7E-3
ZT81	370	12	300	21	1.2E-3
ZT82	370	10	300	21	1-1.4E-3

For use as a contacting layer in an n-i-p configuration the ZnTe must be doped p-type. Therefore we have performed two studies to examine its doping behavior during rf sputtering. The first study used the group IB element, copper, and the second used the group V element, nitrogen. In the first case we achieved the doping by placing small metallic Cu pieces on the target surface. In the second case we used reactive sputtering by mixing small amounts of N_2 into the argon sputter gas. The results are described in Sections 2.2.1 and 2.2.2 below.

2.2.1 Cu Doping--LPVD and rf Sputtering

In our earlier studies of *laser-deposited* ZnTe:Cu,[2] the films were prepared from cold-pressed targets in which the Cu was mixed with the ZnTe in known amounts. The laser deposition was performed on substrates at 300 °C. The copper included in the as-grown film was compared with the Cu fraction of the target and shown to be roughly the same as measured by SEM/EDS with the JEOL model JSM 6100 SEM (within the limits of the EDS technique which we take as ±50% at the 1% Cu level). The film resistivities are shown in Fig. 2-7.

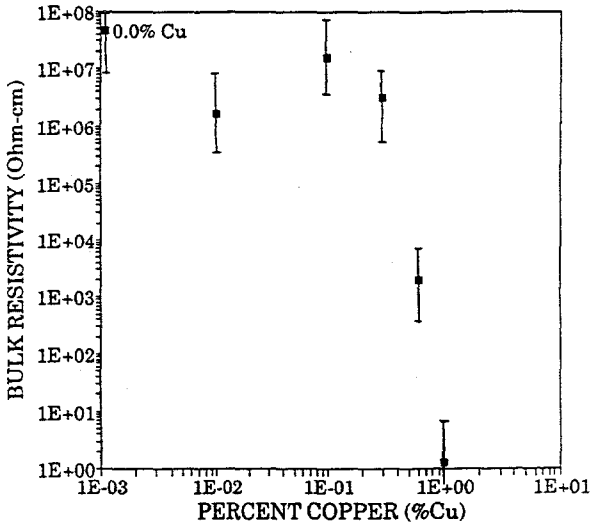

***Fig. 2-7:** Resistivity of ZnTe:Cu films grown by laser deposition from pressed powder targets of CdTe mixed with elemental Cu powder.*

In the studies of *rf sputtered* films, the copper doping level was controlled by adjusting the fraction of surface area which was covered by the Cu. No specially prepared Cu-doped ZnTe targets were used. Films were grown with rf power of 120 W on borosilicate glass at temperatures between 400 and 470 °C. The Ar sputter gas pressure was 12 mTorr. Electrical conductivity and Hall measurements were made on a small piece cut from the center of each ~3 inch square substrate.

Recently Gessert, et al[14] have reported the growth of Cu-doped ZnTe by rf sputtering. For a ZnTe film with 5% Cu, they found a resistivity somewhat less than 0.1 Ω-cm for depositions above 300 C. This is consistent with our sputtered film data of Table 2.2 and with the trends shown in Fig. 2-7 for our LPVD films.

In our rf sputtering studies of Cu-doped ZnTe the Cu content of the films was estimated from EDS measurements. Normalization was done from LPVD films of copper-doped ZnTe (*vide supra*) in which we assumed that the Cu content of the film was the same as that of the pressed powder target mixture. Table 2.2 summarizes the results obtained for several Cu-doped films. For reference we have indicated the surface area covered by the metallic Cu pieces. Note that with a two-inch diameter ZnTe target (20 cm^2), the relative areas of Cu to ZnTe are very small but Cu is known to be a very efficient sputterer and the copper pieces were generally placed at the point of highest sputtering rate on the circular erosion track. It should be noted that the sputtering rate of Cu is very sensitive to the exact position of the Cu piece on the target and this accounts for the poor correlation in Table 2.2 between the Cu area on the target and the EDS measurements of Cu in the film.

The conductivity values reported in Table 2.2 are for in-plane measurements performed at 290 K. Conductivities have errors of typically ±20%. The Hall measurements (in-plane) indicated low mobilities and consequently the errors in mobility and carrier concentration are estimated to be in the range of factors of 2 to 5. Therefore the carrier concentrations shown in Table 2.2

should be considered only as estimates. The mobilities were near the measurement limits, typically from 0.5 - 2 cm^2/V-sec, and showed little dependence on dopant density. Even with this limited set of samples however, one may notice that the electrical activity (σ and n) appears to depend on the growth temperature, with growth at 420 C yielding higher conductivity and carrier density than at 470 C even though the total incorporation of Cu appears to be higher at 470 C. In the case of sample ZT7, there were no pieces of metallic copper on the target but there was a visible discoloration on the target surface surrounding the spot where copper pieces had been placed for earlier depositions. Evidently there was significant sputtering of Cu onto the ZnTe target surface. Apparently there was a small amount of Cu incorporation in the film as shown by the ~5 order of magnitude increase in electrical conductivity above that of pure ZnTe (ZT47) even though the incorporation of Cu was below the detection limit of the SEM/EDS (~0.2 %). The conductivity increases by more than nine orders of magnitude as the Cu content increases. The maximum conductivity is about ten times higher than found by Gessert, et al for 5% Cu target and the maximum hole density is about a factor of 3 higher.

Table 2.2: Sputtered ZnTe dependence on Cu content

SAMPLE ID	Cu area (cm^2)	Cu (wt%-EDS)	T_s (°C)	σ (1/Ωcm)	n(cm^{-3})
ZT47	0	0	400	6 E-8	
ZT7	0*	< 0.2	420	7 E-3	5 E17
ZT5	0.085	0.67	420	0.06	2 E18
ZT6	0.085	1.1	470	0.04	3 E17
ZT11	0.16	0.80	420	20	6 E19
ZT4	~1	6.4	470	100	2 E21

* See text.

Raman scattering provides some information on the film quality and the bonding arrangements of these copper-doped films. Fig 2-8 shows the first and second order Raman signals from a series of three ZnTe films, two of which are copper doped, and a third trace taken from a single crystal of ZnTe:Cu. Note that all of the Cu-doped ZnTe samples show an additional peak at 160 cm^{-1}, which we have not identified, and also a decrease in Raman signal as the Cu content increases. In summary, we find that Cu doping is easily done with rf sputter growth of ZnTe simply by laying metallic Cu pieces on the sputter cathode target. Conductivities up to 100 / Ω-cm are readily achieved.

2.2.2 Nitrogen Doping

Copper is notorious as a fast diffuser in most semiconductors. Thus there is considerable interest in alternative p-type dopants in ZnTe. Recently there has been considerable success in the use of plasma sources for generating atomic N for doping of ZnSe in molecular beam epitaxy (MBE).[15] At least one study has indicated potential for similar doping of MBE-grown ZnTe with atomic N.[16] The rf sputtering system naturally generates atomic and ionic species in the gas

plasma. Therefore we have investigated the possibility of introducing small amounts of N_2 into the Ar sputter gas with the hope of achieving doping in the film. The results have been quite promising although we have not achieved the extremely high dopant levels seen with Cu doping.

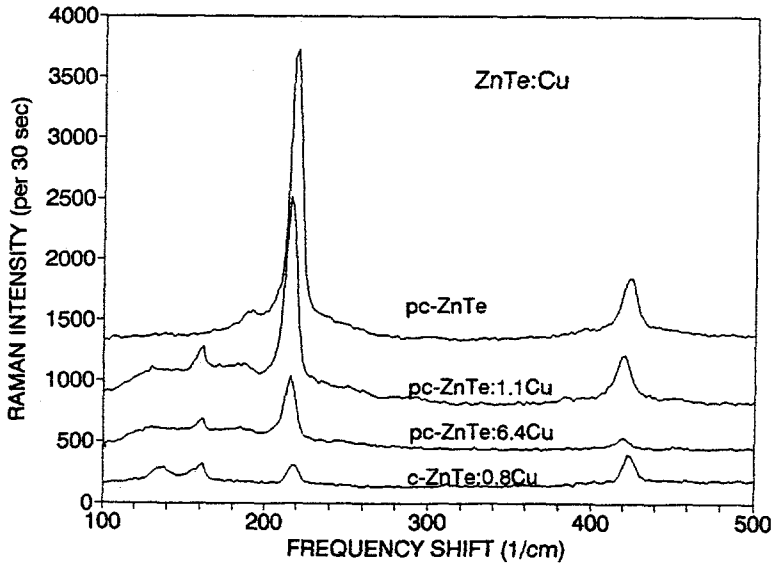

Fig. 2-8: *Raman spectra of several sputtered ZnTe:Cu films. First and second order LO mode of ZnTe are dominant. Small peak at 160 cm^{-1} may be a resonant mode from Cu.*

Table 2.3 presents details of a series of the films grown under a range of N_2/Ar flow rates. The data indicate that it is possible to increase the electrical conductivity from ~5 x 10^{-8}/Ω-cm to as high as 6 x 10^{-2}/Ω-cm. The electrical activity is sensitive to the ratio of N_2 to Ar, but also strongly dependent on the growth temperature with better electrical activity occurring near 400 C than at 300 C. Maximum conductivity is reached at approximately 5% N_2/Ar mixtures for a pressure of 18 mTorr and a substrate temperature of 400 C. Flow rates varied in the range of 10 to 50 sccm. The temperature dependence of the conductivity was measured for many of these films over a limited temperature range from about 0 C to 80 C. The conductivity is described well by a thermal activation model with activation energies shown in Table 2.3. These prelim-

Table 2.3: Reactive sputtering of ZnTe--dependence on N_2/Ar ratio

SAMPLE ID	T_s (°C)	P_{rf}	$N_2/(Ar+N_2)$	E_{act}(eV)	σ (1/Ωcm)
ZT39	300	120	0		
ZT47	400	120	0	0.47	5.7E-8
ZT46	300	120	0		1.4E-5
ZT48	400	150	0.05	0.094	5.9E-2
ZT49	400	150	0.01	0.20	1.3E-3
ZT50	300	150	0.03	0.21	3.7E-4
ZT51	300	150	0.05	0.26	4.0E-4
ZT40	300	120	100		4.8E-6

inary data are sufficient to indicate that, although doping by the addition of partial pressures of N_2 in the sputter gas is quite promising, deposition parameters of substrate temperature and partial pressure must be carefully controlled.

In the case of nitrogen doping of ZnTe, Raman scattering has served as a useful quality control. Fig. 2-9 shows that the vibrational spectra of films grown with 5% partial pressure of N_2 are very sensitive to the growth temperature. At 335 C there is almost no Raman evidence of the usual LO phonon mode of ZnTe; the ZnTe LO phonon is strongest at T_s = 400 C. The spectrum at 430 C is weaker than at 400 C but this arises from the fact that the film thickness was considerably less. At 400 C there appears to be significant amounts of elemental Te in the film (See discussion of Fig. 2-10 below.) but these modes are essentially gone at 430 C.

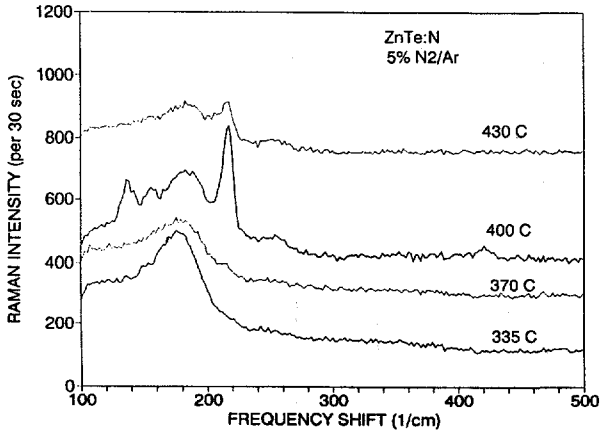

Fig. 2-9: Raman spectra of ZnTe:N films grown at different substrate temperatures. Gas mixture 5% N_2 in Ar; P_{rf} = 150 W.

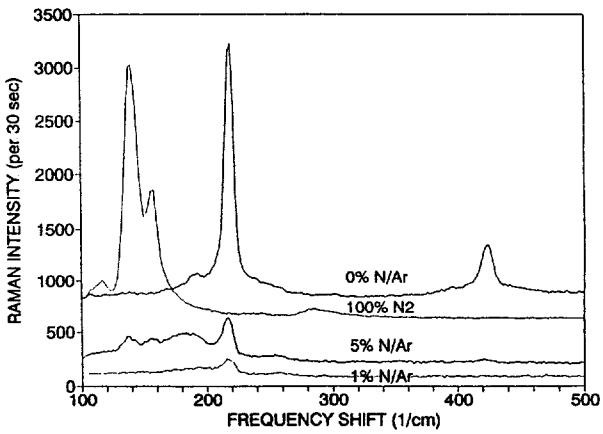

Fig. 2-10: Raman spectra of ZnTe:N grown in N_2/Ar mixtures. T_s=400C except for 100% N_2 where T_s=300C.

Fig. 2-10 shows the Raman scattering behavior of films grown in ambients ranging from pure Ar to pure N_2. For the case of sputtering in pure N_2, the growth rate was substantially lower although the films appeared to have color similar to films grown in pure Ar. However, the Raman spectra show no evidence for ZnTe vibrational modes. Instead the most prominent peaks at 140 and 160 cm^{-1} arise from elemental Te. Pure Te is known to have a very large Raman cross section, however, so that only a few percent of elemental Te could produce the signal observed.[17] The broad peak at ~180 cm^{-1} is likely due to amorphous or microcrystalline ZnTe.

2.3 Laser physical vapor deposition

2.3.1 LPVD chamber modifications

During the past year, the LPVD system has been redesigned in two ways. The target system has been modified to accommodate four two-inch diameter sputtering targets on a large rotatable disc. Each of the targets can be moved, under vacuum, into the center of the disc where the laser

ablation occurs. The previous target arrangement utilized ~0.5 x 1 inch cold pressed targets.[2] The new arrangement achieves much greater target life, allows the use of commercially available hot-pressed sputter targets, and permits much wider scan of the laser beam which leads to better film uniformity. In addition, the substrate holder and heater have been redesigned with the use of two linear quartz-halogen lamps which permits heating in the presence of oxygen and other ambients. Furthermore the substrate holder, which is not coupled to the heater assembly, is rotated. The combination of these changes yields much greater uniformity in the film deposition. With the modified system the films have typically less than 20% thickness variation over the center three-inch diameter.

The modified system has been used mainly for the deposition of $CdCl_2$ layers in the fabrication of solar cells. (We continue to use LPVD for the $CdCl_2$ deposition rather than $CdCl_2$/methanol solution application because it gives much better thickness uniformity and more reproducible cell performance across the typical 2.5 inch square area over which cells are fabricated.) We find that for our 1.5-2.0 μm thick CdTe layers, the $CdCl_2$ layer must be ~0.4 μm to achieve optimum performance.

2.3.2 LPVD growth of CdTe doped with O and with Cu

With the redesigned heater system it has been possible to deposit films in the presence of oxygen. We have deposited individual films on borosilicate glass and also fabricated complete solar cells in the LPVD chamber (using laser deposition for CdS, CdTe and $CdCl_2$).

In order to test for possible electrical activity of oxygen, films were first deposited on borosilicate glass (Corning 7059 and NEG 0A-2). We found only a small decrease in resistivity for growth in O_2. The CdTe resistivity dropped from 3 x 10^7 Ω-cm to 6 x 10^5 Ω-cm. Some change was also observed in the photoluminescence at 80K which indicates that there is some activity from possible oxygen doping. For growth in O_2 the as-grown films showed little PL but after a 400 C anneal for 20 minutes, substantial near-band-edge PL (λ ~ 790 nm) and deep level PL (λ ~ 860 nm) was observed. This contrasts with the situation for CdTe films grown in vacuum ($p \leq 2 \times 10^{-6}$ Torr) where no PL was observed even after annealing (without a prior application of $CdCl_2$). This behavior is shown in Fig. 2-11.

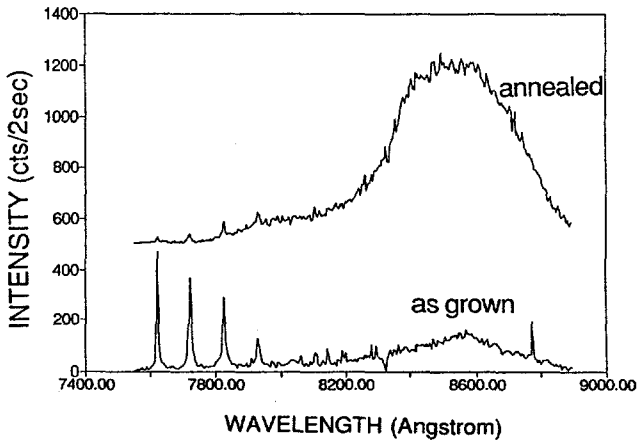

Fig. 2-11: Raman and PL from LPVD CdTe film grown in $9x10^{-5}$ Torr of oxygen. Baseline raised by 500 cts for annealed spectrum. λ=752 nm, T= 80 K.

Additionally, a preliminary study was made of Cu doping of CdTe. In this case we observed significant PL in the as-grown films which remained after 400 C anneal in air. (See

Fig. 2-12.) The film resistivity dropped substantially from 10^8 Ω-cm to 2 x 10^5 Ω-cm when approximately 2% Cu was mixed into the cold-pressed CdTe target. These copper-doped films are now being used for cell fabrication.

For comparison, Fig. 2-13 shows the typical PL signal observed from an LPVD CdTe film grown with no background of O_2 in the chamber during growth ($p < 5 \times 10^{-6}$ Torr.) The fact that the as-grown film shows multiple-order phonon Raman lines (first, second, and third) indicates reasonably high film quality. After annealing there is some improvement in film quality and/or grain size as evidenced from still higher-order Raman lines and the beginnings of a photoluminescence band near 7900Å. However, in contrast with the films grown in O_2 or with Cu doping the PL is weak. After $CdCl_2$ treatment, a dramatic increase in PL intensity occurs as described in Section 2.3.3 below.

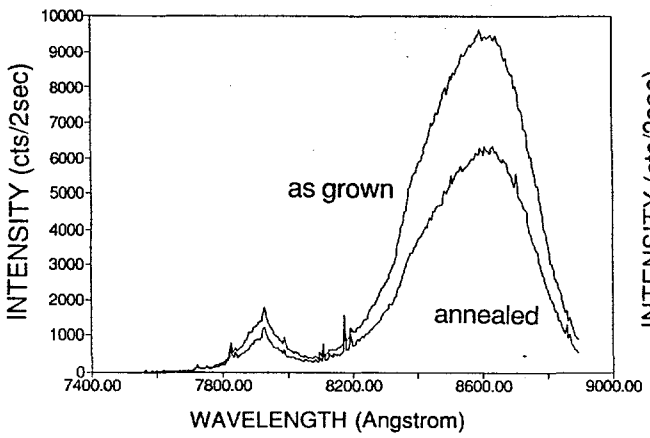

Fig. 2-12: Raman and PL from LPVD CdTe films grown with elemental Cu in the target. λ=752 nm, T = 80K.

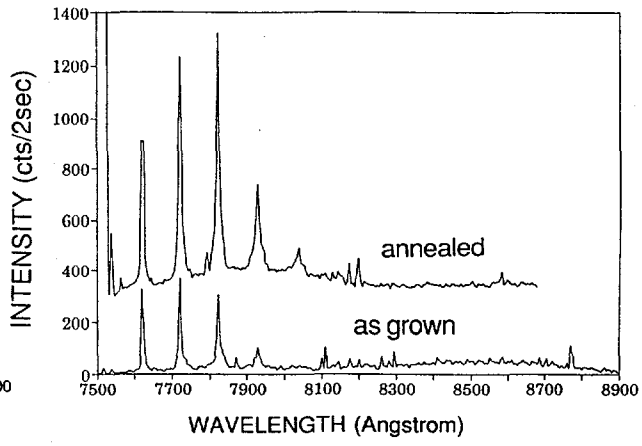

Fig. 2-13: Raman spectrum from LPVD CdTe grown without O_2 or Cu. λ=752 nm, T= 80 K.

2.3.3 Interdiffusion in cells with CdTe:O

When solar cells were prepared with these films grown in oxygen, the principal effect was that the CdTe layer could be grown thicker (up to ~2 μm) before deterioration of the cell performance. This is consistent with the observed increase in dark conductivity. Figs. 2-14a,b show the performance of a number of 0.11 cm^2 cells in which all three depositions (CdS, CdTe, and $CdCl_2$) were made by LPVD. The cells of Fig. 2-14a used a CdTe layer which was grown in a background of O_2 ($p = 5 \times 10^{-4}$ Torr). A smaller number of cells were grown under the usual vacuum conditions ($p \leq 5 \times 10^{-6}$ Torr). It was found that best results were obtained after first growing about 300 nm in high vacuum conditions ($p \leq 5 \times 10^{-6}$ Torr) and then introducing O_2 at 0.1 mT for the remainder of the film growth. Other groups have found that some addition of oxygen during the CdTe growth[18] is beneficial to the cell performance. However, the effect of oxygen on the LPVD growth of CdTe is not yet well understood. Further discussion of the effects of O_2 is presented in Section 3.1.3 below.

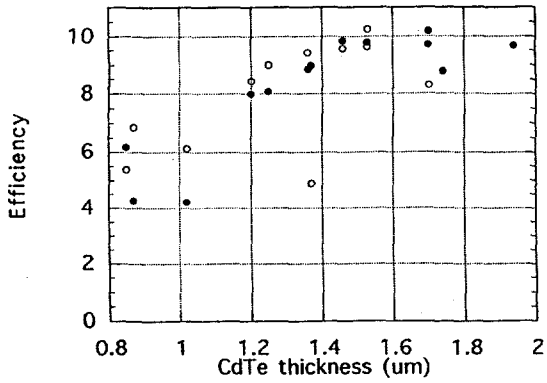

Fig. 2-14a: AM1.5 efficiency of LPVD cells with CdTe grown in 5 x 10^{-4} T of oxygen. • = 30 min. anneal; O = 20 min. anneal.

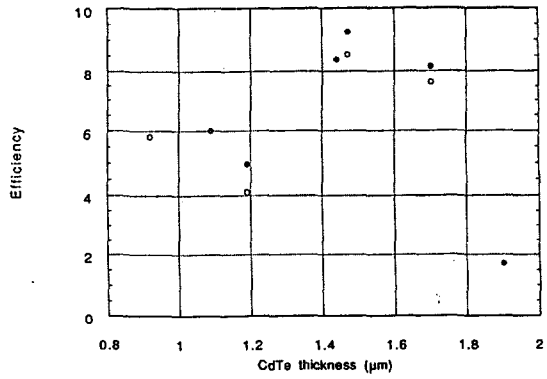

Fig. 2-14b: AM1.5 efficiency of LPVD cells with CdTe grown in vacuum (p<5x10^{-6}T). • = 25 min. anneal; O = 15 min. anneal.

We have obtained some evidence that the presence of small quantities of oxygen in the CdTe film may retard interdiffusion across the CdTe/CdS interface. The principal evidence comes from PL studies from finished solar cells. Using the 752 nm Kr laser line and the sample at ~80K, one can excite PL from either the CdTe-air interface or from the CdTe/CdS interface. Figure 2-15a shows the near-band-edge spectra from cells with CdTe grown in vacuum for four cases (two different interfaces and two different solar cell anneal times). Figure 2-15b shows the corresponding case for cells grown in 0.5 mTorr of O_2. Note that for vacuum-grown cells there is a red shift of 100 - 140 Å of the near-band-edge peak when observed from the CdTe/CdS interface. This undoubtedly results from S and Te diffusion across the interface as observed by Clemminck et al[19] and by Oszan & Johnson.[20] It is known that the band edge of the alloy

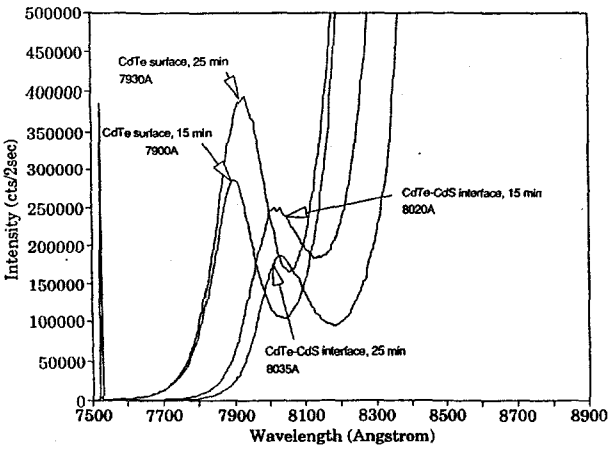

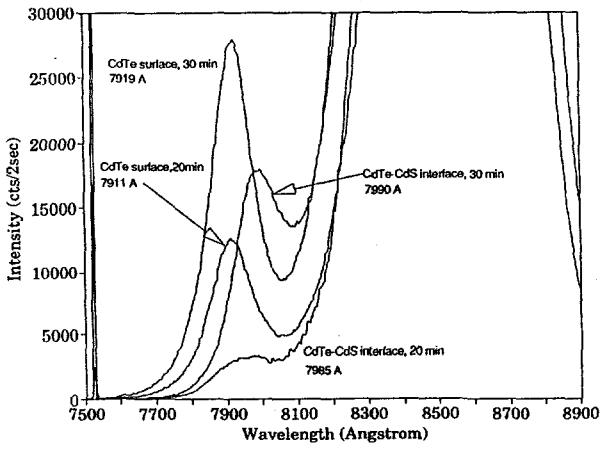

Fig. 2-15: 77K photoluminescence produced by 752.2 nm excitation from LPVD CdTe layers in solar cell structures after treatment with $CdCl_2$ and annealing in air at 400 °C for different times. a) CdTe grown in vacuum; b) CdTe grown in 5 x 10^{-4} Torr of O_2. Results are shown for both CdTe/air interface and for the CdTe/CdS interface.

CdS_xTe_{1-x} for small x is reduced from that of CdTe.[21] Since this near-band-edge PL peak probably tracks the band edge, these data indicate interdiffusion as a result of the anneal treatment at 400 °C in air after $CdCl_2$ deposition. In addition Fig. 2-15a shows that for the longer anneal time, some PL shift is also observed at the CdTe air interface. Other data indicate that the peak shift increases with time up to about 30 minute anneals. In the case of cells grown in O_2, a similar but smaller shift is seen in PL from the interface. However, there is no evidence of any red shift in PL observed from the CdTe-air interface. The data may point to an important role for oxygen in CdTe as a diffusion inhibitor when cells are treated with $CdCl_2$ and annealed in the presence of O_2. It may be that O has its strongest effect inhibiting diffusion along grain boundaries. Further work is in progress to clarify the role of oxygen during growth.

2.4 Difficulties with blistering of CdTe on CdS

One of the difficulties we have encountered during the past year was the occurrence of small bubbles or blisters which sometimes occur on CdTe films grown on CdS. This problem does not arise for CdTe films grown directly on SnO_2-coated soda-lime glass or for films grown on borosilicate glass (Corning 7059 or NEG 0A-2). The blistering occurs only during the annealing after treatment with a layer of $CdCl_2$. We have determined that the blistering is concentrated near the center of the film which is directly above the center of the sputtering target. Thus the problem is apparently aggravated by some process in the sputtering chamber--possibly from electron or neutral atom impacts. However, exposure to ambients *ex situ* between the CdS deposition and the CdTe deposition appears also to contribute to the problem.

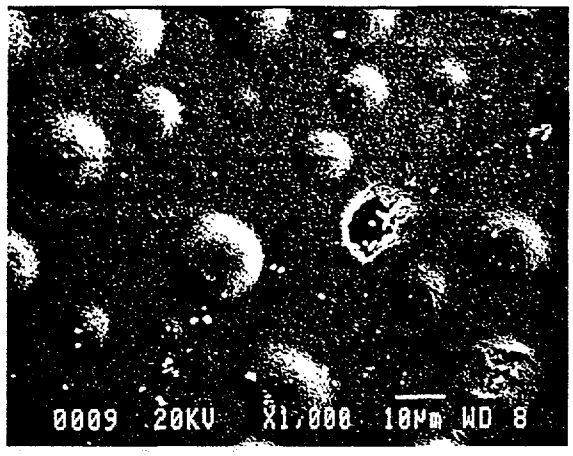

Fig. 2-16: *SEM micrograph of cell showing severe blistering after $CdCl_2$ treatment and 400°C annealing in air.*

We anticipate that this recurring problem will be controlled as we begin operation of a new sputtering chamber which will utilize two planar magnetron guns and permit sequential deposition of CdS and CdTe without breaking the vacuum and without temperature cycling of the substrate. Figure 2-15 shows the typical size and pattern of blisters when they do occur.

3.0 Advances in Materials Characterization and Growth Diagnostics

As described earlier in this report and in previous annual reports, we maintain a considerable range of capability in the area of materials characterization, device testing and growth diagnostics. Thus we regularly characterize the individual films using x-ray, scanning electron microscopy with x-ray analysis (SEM/EDS), temperature-dependent electrical measurements including the Hall effect, double-beam optical absorption, and Raman scattering and photoluminescence. For device testing we utilize I/V and spectral quantum efficiency measurements as well as optical or light beam induced currents (OBIC or LBIC). Many of these

materials-characterization and device-testing measurements have been highlighted in the previous discussions in this report. During the past year, however, some new measurement systems have been added and other capabilities have been enhanced. These are described in more detail below. We shall discuss new experimental capabilities in

1. photoreflectance and electroreflectance (PR and ER), and
2. scanning tunnelling microscopy (STM).

We have enhanced our capabilities in the area of Raman and photoluminescence through the addition of

3. a new CCD detector for the Raman/PL system, and
4. the instrumentation of a diode laser system for resonant Raman and PL excitation spectroscopy.

Finally, we present some early diagnostic measurements of the rf sputtering system by

5. optical emission spectroscopy (OES) with a vidicon array detector.

3.1 Photoreflectance and electroreflectance studies of CdTe interfaces

The electrical and optical properties of CdTe interfaces are critical in the performance of the CdS/CdTe solar cell. The cell properties are dominated by the CdS/CdTe junction region. Also the electrical behavior of the backside contact to the CdTe is extremely important. Modulated reflectance spectroscopy is well known as a sensitive probe of interfaces and we have implemented over the past year two versions of reflectance spectroscopy--photoreflectance and electroreflectance. These techniques are particularly valuable for studying semiconductor properties near the fundamental band gap and at other critical points in the valence-to-conduction-band joint density of states. In cases for which contact formation is possible, such as in completed solar cells, electroreflectance is easily applied. However, photoreflectance has the advantage of being easily applied to free surfaces as well as some interfaces which lie below window layers of wider band gap semiconductors. Although we have demonstrated successful application of PR at the fundamental band edge of CdS, we have emphasized work at the fundamental gap of CdTe and will summarize that work below.

3.1.1 PR and ER Instrumentation

The system uses a tungsten-halogen lamp with a 1/4 meter SPEX monochromator for the reflectance source. The reflected signal is detected by a silicon photodiode, amplified by an Ithaco 164 current sensitive preamplifier and detected through an Ithaco Dynatrac 391A lock-in analyzer. In the case of solar cells, modulation is provided simply by applying a square-wave signal across the cell terminals. For photoreflectance, the modulation is provided by either a Kr ion laser at 647 nm or 752 nm or an argon laser at 514 nm. A HeNe laser could also be used. Modulation was provided by a chopper wheel with the reference signal input into the lock-in. The system layout is shown in Fig. 3-1. Typically the monochromator was operated with a resolution of 1 nm, with the output beam focussed to a roughly square 3 mm shape on the film or solar cell.

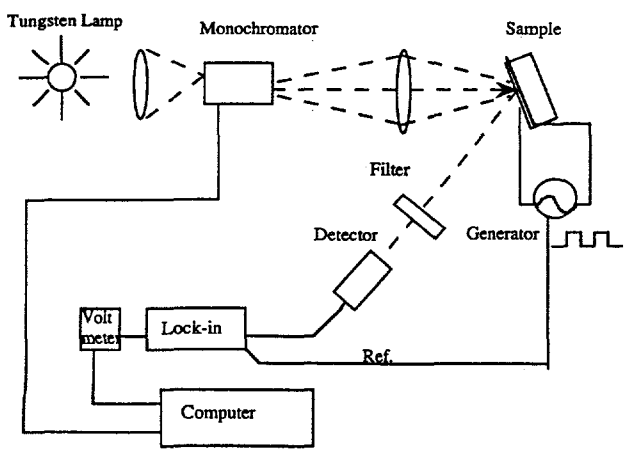

Fig. 3-1a: Electroreflectance set-up.

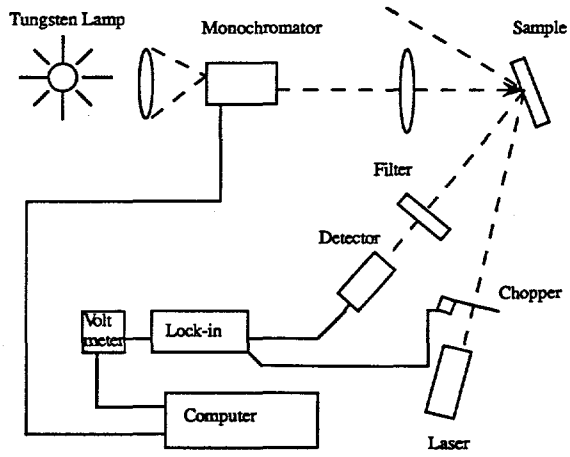

Fig. 3-1b: Photoreflectance set-up.

3.1.2 Photoreflectance from sputtered CdTe films

We have studied the photoreflectance of several rf sputtered CdTe films grown on NEG glass at different substrate temperatures. The PR data are shown in Fig. 3-2 which compares three as-grown films deposited at 240, 380, and 450 °C. The films were grown at an Ar pressure of 18

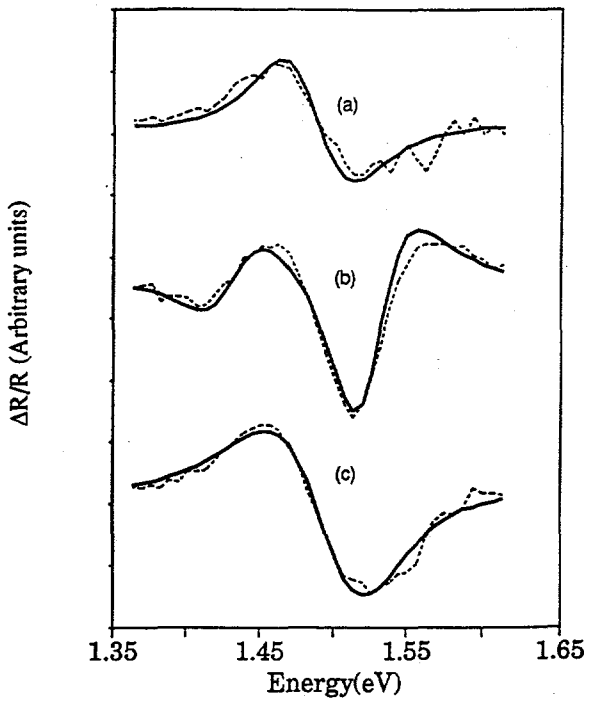

Fig. 3-2: PR spectra for as-grown sputtered CdTe films deposited at a) 240 C, b) 380 C, and c) 450 C. Dotted/solid lines are expt'l data/TDFF fits.

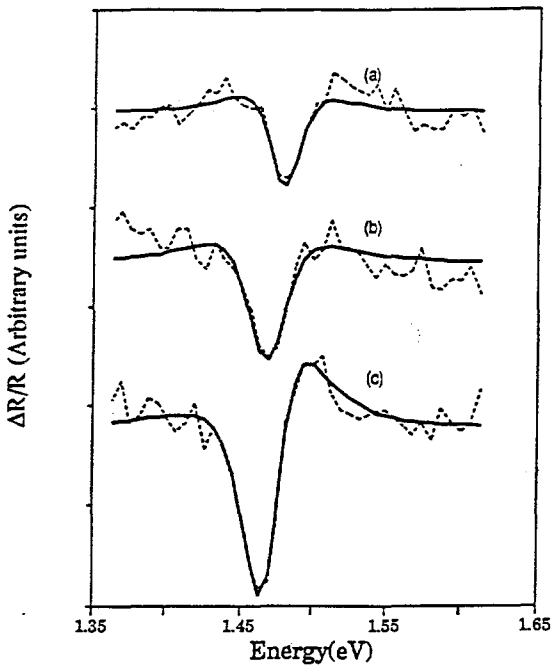

Fig. 3-3: PR spectra of same sputtered CdTe films as for Fig. 3-2 after $CdCl_2$ treatment and 400 C anneal.

mTorr and an rf power of 120 W. In general higher quality films will have narrower lineshapes in PR and this is seen to occur at a growth temperature of 380 °C. The solid curves in Fig. 3-2 are fits to the third derivative functional form (TDFF) of Aspnes as described below.

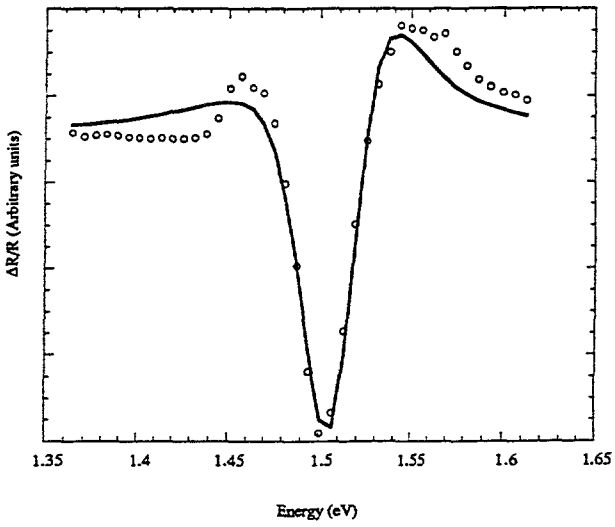

Fig. 3-4: PR spectrum of single crystal CdTe (circles) with best TDFF fit (solid line).

After these films have undergone the standard $CdCl_2$ deposition (by LPVD) and an air anneal at 400 °C for 15 min, the PR signal was measured again. The results after anneal are shown in Fig. 3-3. One may observe that the linewidth is reduced and the line center is shifted to *lower* energy. Finally, for reference, we show in Fig. 3-4 the PR signal from the <100> surface of a high quality single crystal of CdTe which had been etched in a 0.05% Br/methanol solution for 5 seconds shortly before the data were acquired. In all cases the fits have been made to the TDFF functional form discussed below.

Aspnes[22] has shown that the low-field (electro- or photo-) modulated reflectance signal near a three-dimensional critical point such as at the direct gap of CdTe at the Brillouin Zone center, should have the functional form:

$$\Delta R/R = \begin{cases} C[(E-E_g)^2+\Gamma^2]^{-5/4}\cos\{\theta-(5/2)\tan^{-1}[\Gamma/(E-E_g)]\}, & E<E_g \\ C[(E-E_g)^2+\Gamma^2]^{-5/4}\cos\{\pi/2+\theta-(5/2)\tan^{-1}[\Gamma/(E-E_g)]\}, & E>E_g. \end{cases} \quad \text{Eq. (4)}$$

The phase θ is related to the dimensionality of the critical point and to the electron-hole interaction; E_g is the energy gap with damping Γ. This functional form was numerically fit to the observed signals and values of the fit parameters were extracted. The fitting parameters thus obtained are shown in Table 3-1. Similar results have been obtained by Rodrigues, et al[23] for an epitaxial layer of CdTe.

The first point to notice is that for the as-grown films, the film grown at 380 °C displays the highest energy gap (E_g=1.515 eV) and the lowest broadening parameter (Γ=42.6 meV). After treatment with $CdCl_2$ and air anneal of these films, all three films show a *decrease* in the energy gap ($E_g \cong$1.47 eV) and a decrease in the broadening parameter (Γ=25-32 meV). One of the films has a PR linewidth which is slightly less than the single crystal sample. Some decrease in the PR linewidth may result from probable grain growth during the anneal treatment. However, the shift in E_g cannot easily be explained by grain size effects. Possibly a slight change in stoichiometry during anneal may shift the band edge. Further work needs to be done to identify the source of this shift.

Table 3.1: Critical Point Energies, Broadening Parameters, and Relative Amplitudes for Photoreflectance from Sputtered CdTe Films					
Sample	**Substrate Temp. (°C)**	**Amplitude C**	**E_g (eV)**	**Γ(meV)**	**Phase θ(rad.)**
CT-26	240	3.29×10^{-5}	1.497	67.5	1.195
CT-24	380	8.42×10^{-6}	1.515	42.6	0.619
CT-25	450	2.95×10^{-6}	1.485	62.1	0.566
CRYSTAL		1.63×10^{-4}	1.509	32.8	-0.327
CT-26 ann	240	3.06×10^{-5}	1.470	31.2	-0.174
CT-24 ann	380	1.87×10^{-5}	1.468	32.7	-0.826
CT-25 ann	450	6.00×10^{-6}	1.479	25.3	-0.888

3.1.3 Electroreflectance at the CdS/CdTe interface

The modulated reflectance observed in response to optical pumping with the chopped laser beam is understood to result from changes in the band bending at interfaces due to carrier generation in regions of strong electric field. These often result from depletion regions at surfaces and from built-in electric fields due to carrier diffusion across interfaces. In the case of the solar cell, however, the fields may be modulated directly through the application of small modulated bias voltages. Thus, we have studied the CdS/CdTe interface in the solar cell with electroreflectance.

Figure 3-5 shows the ER signal from four solar cells with different performances. The V_{oc} ranged from 0.28 V to 0.77 V. Note that the ER signal amplitude correlates strongly with the cell open-circuit voltage and efficiency.

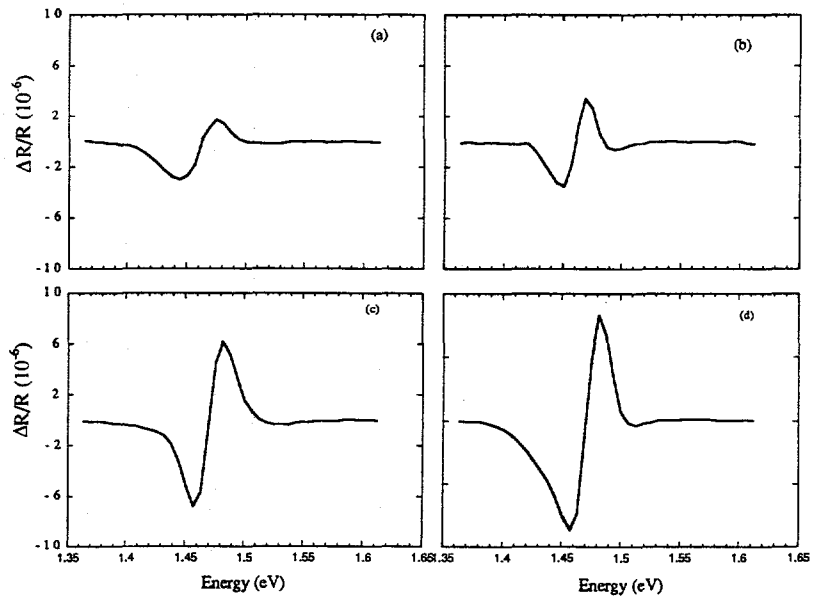

Fig. 3-5: ER spectra from CdTe/CdS solar cells with different performance.
a) V_{oc}=0.28V, I_{sc}=1.83 mA;
b) V_{oc}=0.53V, I_{sc}=1.80 mA;
c) V_{oc}=0.63 V, I_{sc}=1.80 mA;
d) V_{oc}=0.77 V, I_{sc}=2.17 mA.

The fitting parameters which give a good fit of the TDFF form to the observed ER spectra are shown in Table 3-2 together with the solar cell parameters V_{oc}, and I_{sc}. Note that the values of E_g from the fit are nearly the same as those of the annealed individual CdTe films. (Both cells and the annealed films were treated with $CdCl_2$ and annealed at 400 °C.) The narrowest lineshapes and largest ER amplitudes appear to correlate well with the highest open circuit voltages.

Table 3.2: Electroreflectance Parameters and Solar Cell Performance

Sample	V_{oc} (V)	I_{sc} (mA)	E_g (eV)	Γ (meV)	Rel. Amplitude
scn21.c6	0.28	1.83	1.454	30	6.23×10^{-6}
scn21.c5	0.53	1.80	1.459	26	2.64×10^{-6}
scn21.c22	0.63	1.83	1.469	23	7.66×10^{-6}
scn20.c13	0.77	2.17	1.469	22	1.28×10^{-5}

Finally, we make a direct comparison between the signals from PR with those from ER. Figure 3-6 shows these results obtained from a solar cell. Here the PR signal was obtained with the reflectance beam and the modulating beam incident on the CdS/CdTe interface through the glass/SnO_2/CdS layers. It is readily apparent that the PR signal is quite similar in phase to the ER signal obtained with a small foward bias modulating voltage. This is expected since the incident modulating light beam causes the cell to enter forward bias.

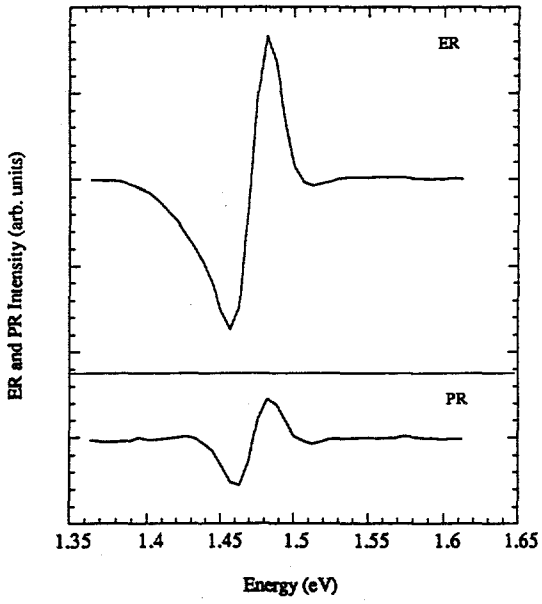

Fig. 3-6: *Comparison of ER and PR signals obtained from two solar cells with 9% efficiency. PR is obtained from the CdTe/CdS interface and ER is for forward-bias modulation.*

In Section 2.3.3 we presented photoluminescence evidence of interdiffusion between CdS and CdTe layers which occurs during the $CdCl_2$ treatment and subsequent anneal and preliminary evidence that growth of CdTe in the presence of O_2 tends to inhibit this interdiffusion. We have studied the same cells also by ER and find results which are consistent with the interpretation of the PL studies given in Section 2.3.3. Figure 3-7a shows the ER signals obtained from a cell grown with minimal O_2 in the LPVD chamber. Note that a significant red shift occurs of the ER resonance with the longer anneal time. By contrast Figure 3-7b shows that for the cell grown in 0.1 mT of O_2 there is very little shift of the E_0 resonance. These results compare favorably with the PL data shown in Fig. 2-1 and appear to confirm the influence of O_2 during the LPVD

2-1 and appear to confirm the influence of O_2 during the LPVD growth as an inhibiting factor in this interdiffusion of Te and S across the CdS/CdTe interface during 400 C anneal after treatment with $CdCl_2$.

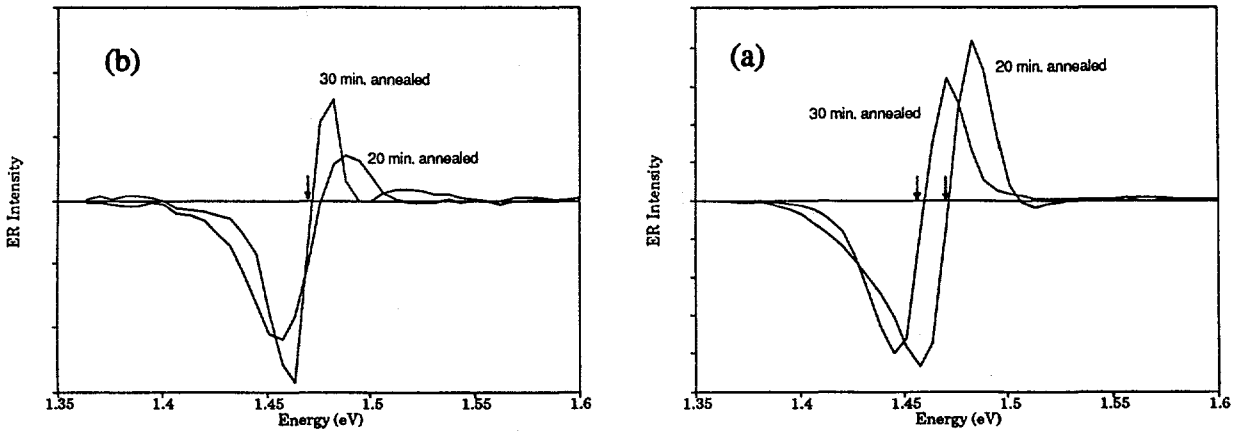

Fig. 3-7: Comparison of ER signals from a) cell grown with O_2 pressure of 1 x 10^{-5} T and b) cell grown with O_2 pressure of 1 x 10^{-4} T for 400 C anneals in air of 20 min and 30 min. Arrows indicate the position of the E_o resonance.

3.2 Scanning tunnelling microscopy

In the last couple of months of Phase Three the University of Toledo acquired a Burleigh ARIS-2200 scanning tunnelling microscope (STM). The scanning head operates under ambient conditions with an x-y scan range of approximately 3 μm square and a z range of about 1.2 μm. Our initial studies indicate that this instrument can provide important useful information about surface morphologies of the various layers of the solar cell--SnO_2, CdS, and CdTe. Both SnO_2 and CdS have sufficient surface electrical conductivity to be observed directly with the STM. For observations of CdTe surface morphology we found that a coating of about 20 Å of gold was

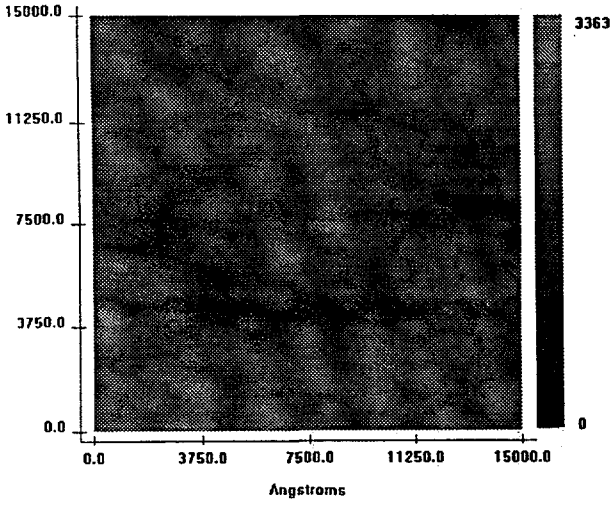

Fig. 3-8a: STM image of LPVD CdS on Corning 7059 grown at T_s=350 C. Mean thickness is 4000Å.

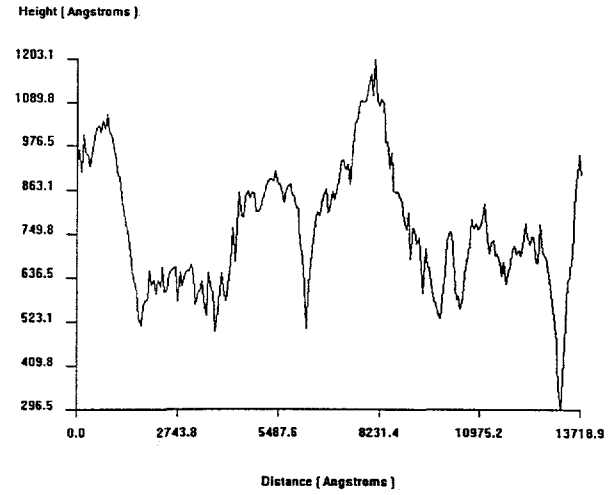

Fig. 3-8b: Cross-section trace from image of Fig. 3-8a taken at y=7500Å.

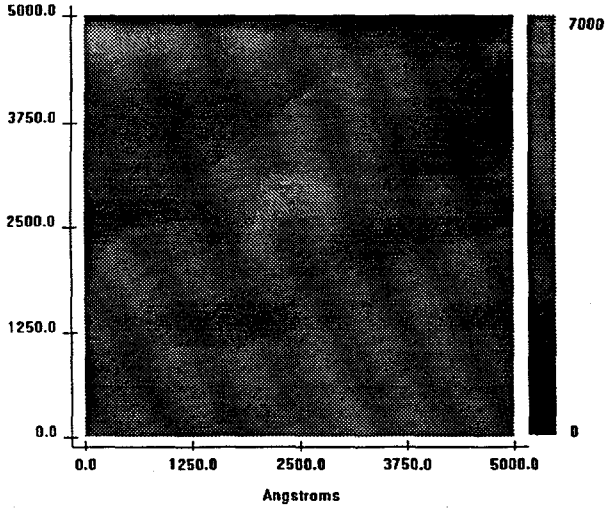

Fig. 3-9a: STM image of CdTe surface of a ~2.2 μm thick solar cell after coating with 25 Å of gold. Cell has been $CdCl_2$-treated and annealed.

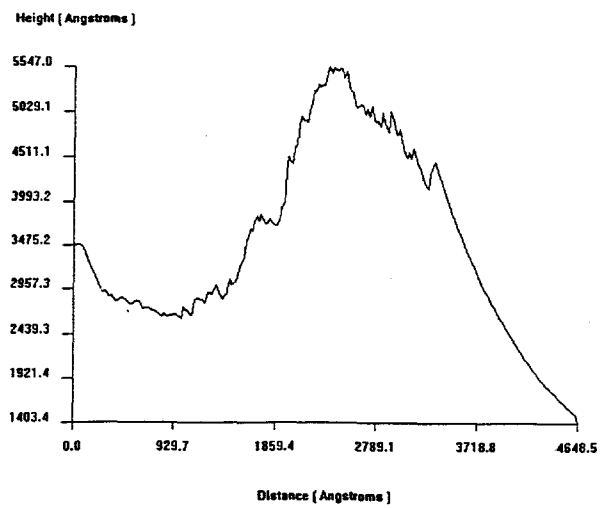

Fig. 3-9b: Cross-section trace from image of Fig. 3-9a taken at y=3750 Å.

sufficient for obtaining good tunnelling signals. The STM measurements complement our SEM studies and can provide more detailed monitoring of changes in grain size and the general surface morphology for different growth conditions (substrate temperature, rf power, etc) and after $CdCl_2$ application and air anneal at ~400 °C. Examples of images are provided in Figures 3-8 and 3-9.

3.3 A new CCD detector for the Raman/PL system

During the past year we have added a CCD detector (Princeton Instruments 298x1152 pixels) to the ISA S3000 triple spectrometer which is used for Raman scattering and for photoluminescence studies. The multiplex advantage of the CCD over the photomultiplier system yields a great increase in speed of data acquisition. In addition, the CCD has a response out to the limit of the Si diode response (~1050 nm) in comparison with the GaAs photocathode PMT (Hamamatsu R943-02) which had good response out to 850 nm only.

The advantage of the CCD has permitted us to use simple, single-mode diode lasers for Raman and PL studies of CdTe.[24] Fig. 3-10 provides an example of Raman and photoluminescence excitation spectra obtained with the diode laser for five different wavelengths from 7766.4 Å to 7789.1 Å. For the CdTe sample held at liquid helium temperature this range of wavelengths tunes through the free exciton position in CdTe and through several bound exciton states.[25] One may observe a peak at 1.5783 eV which resonates strongly in this region. Other impurity-bound exciton peaks may be seen near 1.590 eV which, however, do not appear to be significantly enhanced in this region. The phonon Raman peak is indicated by an arrow in each trace. Wavelengths of commercially available single-mode diode lasers permit us to obtain PL excitation spectra and resonant Raman scattering over the entire near-band-edge region of CdTe. We have obtained a few such spectra from CdTe thin films and solar cells and expect to use this excitation spectroscopy to study near-band-edge defect states.

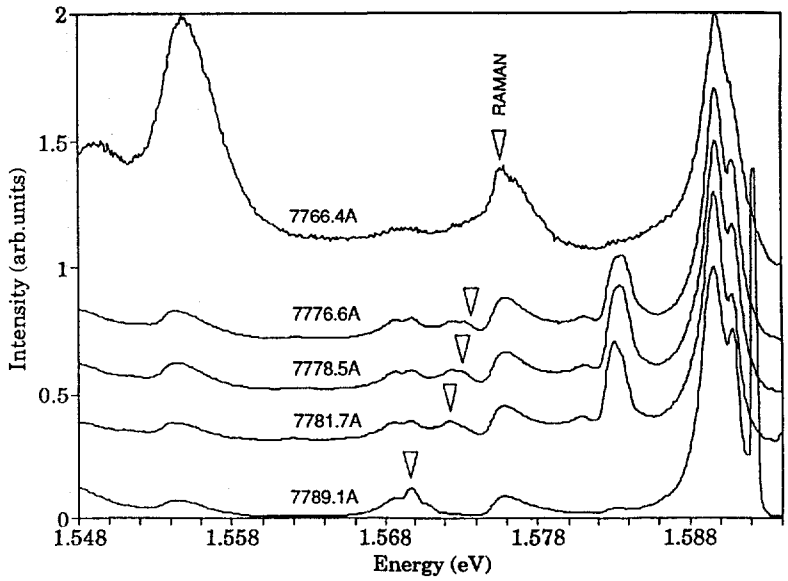

Fig. 3-10: *Photoluminescence spectra obtained at 20K from single crystal CdTe using a small, single-mode diode laser at five different wavelengths in the region of the free exciton. Arrows indicate the Raman peak shifted by 21 meV from the laser line.*

3.4 Optical emission spectroscopy (OES) of the rf plasma

In order better to understand the physics of the planar magnetron sputtering process, we have begun a series of measurements of the optical emission from the plasma. Using an optical fiber bundle to couple light into a 1/4 meter spectrometer (Aries FF250) and a vidicon detector (PAR OMA-II), we have monitored a series of emission lines from ArI, ArII, CdI, CdII, TeII, SI, and SII as a function of gas pressure, rf power, and distance from the magnetron sputter gun. Some preliminary results are given below in Figures 3-11 and 3-12. The limitation of OES is that one can monitor only the emission from excited state species and no information is available directly about ground state species. Nevertheless the method can provide a good monitor of contamination in the system--e.g., H_2O vapor, O_2, and impurities in the sputter target. In addition the spectra provide information on the fraction of ionic species which may impinge on the growing film surface.

Figure 3-11 shows the emission intensity of four neutral and ionized species in the plasma as a function of distance from the sputtering gun. Note that the substrate is 70 mm from the gun. Note that the neutral CdI intensity falls more slowly than the ionized species, ArII & TeII, or the neutral ArI.

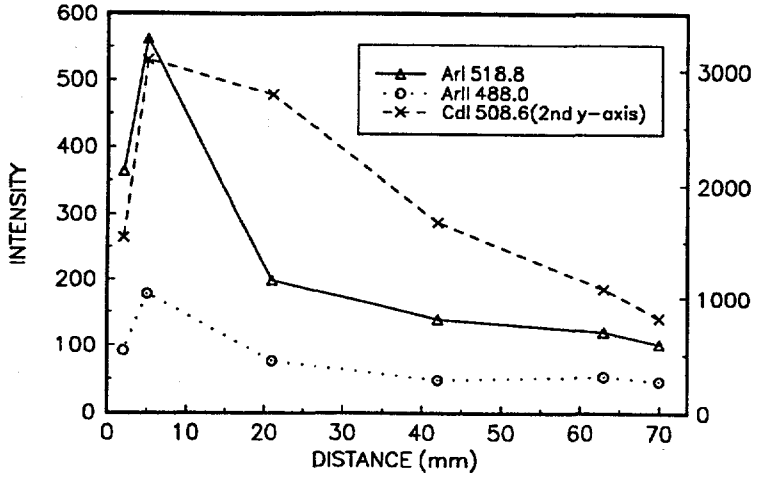

Fig. 3-11: *Emission intensity vs. distance from sputter gun for three species. Rf power 300 W; p = 18 mTorr.*

Figure 3-12 shows the emission intensity of the same four neutral and ionized species at the substrate position as a function of the rf power into the sputter gun. Although the neutral CdI intensity increases monotonically with increasing rf power, the ArI, ArII, and TeII intensities show little increase above 150 W of rf power.

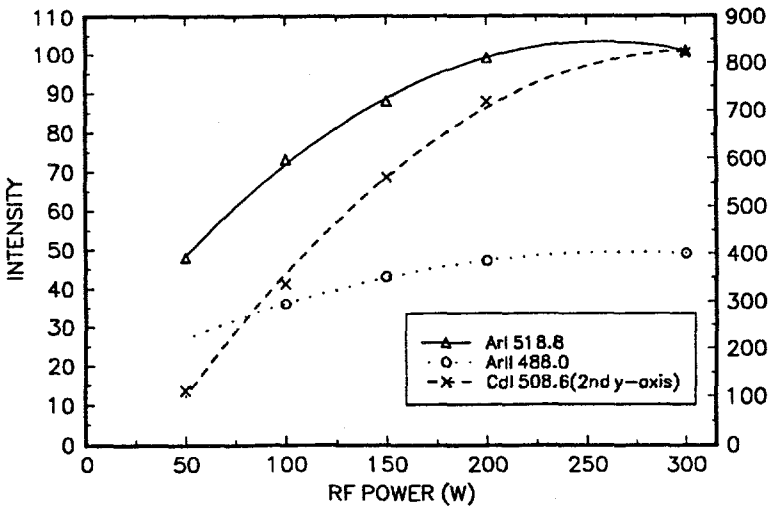

Fig. 3-12: Emission intensity for three species vs. rf power 70 mm above two-inch planar magnetron sputter gun. Argon pressure = 18 mTorr.

4.0 Summer NSF-REU Project

During the summer of 1993, the University of Toledo Department of Physics and Astronomy hosted 16 undergraduate students participating in research projects as part of the NSF-sponsored Research Experiences for Undergraduates (REU) Program. One of these students Craig Hoff, supported by the NSF program, participated in our photovoltaics work. Craig teamed with graduate student Andreas Fischer in an extensive series of measurements of the effect of the presence of oxygen during LPVD growth of CdTe. For this work, he learned to use the excimer laser and the LPVD growth chamber to grow films of CdTe on borosilicate glass and also to grow complete solar cell structures which required laser depositions of CdS, CdTe, and $CdCl_2$. He then determined the electrical resistivity of the CdTe films on glass using a four-point probe, assisted with Raman and PL studies of the films and solar cells, and measured the electrical performance of the cells. His results have already been discussed in Sections 2.3.2 and 2.3.3 above. As a result of his work we expect to extend to rf sputtering the studies of the influence of oxygen during growth.

5.0 Conclusions

Fundamental studies of rf sputtering of CdTe have been done to examine the dependence of the film growth rate on a) substrate temperature, b) rf power, c) sputter gas pressure, and d) erosion condition of the sputter target. We have found that for a deeply eroded target the film quality and solar cell performance is equivalent to that for a fresh, planar target. However, the growth rate may be up to a factor of 1.8 times larger for a deeply eroded target. For our configuration (two-inch target and ~three-inch target-substrate separation) the maximum growth rate occurs for a gas pressure of ~10 mTorr and rf power of 300 W, although only a small increase in growth rate is observed between 200 and 300 W.

Some difficulties with blistering of the CdTe film have been observed in which the CdTe separates from the CdS after the $CdCl_2$ treatment and 400 C air anneal. Recently this has been

a frequent occurrence and appears to be related to details of the rf sputtering of CdTe, possible contamination of the CdS surface between CdS deposition and CdTe deposition, and possibly to the CdS quality. We have prepared many cells with efficiencies > 10% which are completely free of blisters, so the problem does not appear to be intrinsic to the rf sputtering process, although we have not yet fully identified the source of the problem.

Rf sputtering of ZnTe has been done and successful doping with Cu has been done by simply laying metallic Cu pieces onto the surface of the ZnTe target (our system uses a "sputter-up" configuration). In addition reactive sputtering with N_2 has shown considerable promise with resistivities as low as 20 Ω-cm achieved. Raman scattering has shown that substrate temperature is important for optimizing the reactive sputtering with nitrogen.

Preliminary studies of laser physical vapor deposition growth of CdTe in the presence of O_2 indicate significant effects. The resistivity can be reduced by a factor of ten or more; the photoluminescence signal can be increased considerably; and slightly thicker layers can be used for the solar cells.

A variety of results of materials characterization have been presented--scanning electron microscopy with energy dispersive x-ray spectroscopy, Raman and photoluminescence, as well as electrical conductivity and Hall measurements. In addition we have presented results from a new system for electroreflectance and photoreflectance measurements, resonant Raman and PL with a diode laser, and first results from a scanning tunneling microscope. Some early results have been shown for optical emission spectroscopy of the rf sputtering plasma.

6.0 Future Directions

We shall continue to emphasize work on understanding the physical processes underlying the rf planar magnetron sputtering of II-VI semiconductors and optimizing their performance for PV. This will include optical emission studies during the growth process, substrate temperature dependence, rf power dependence, and gas pressure dependence. With a new two-gun sputtering chamber we are able to do two sequential depositions without exposure to air and without substrate cool-down between depositions. In addition, we expect to include studies of substrate electrical bias effects and the effects of adjusting the magnetic fields of the planar magnetron sputter guns.

Preliminary results on the role of oxygen in laser-deposited films will be pursued and the results extended to rf sputtering. Further work with the LPVD system will include studies of alloy growth and their incorporation in solar cells.

Attention will be given to developing contacting designs other than the Cu/Au contacts to the CdTe which we have used up to the present time.

7.0 Acknowledgments

Many individuals in addition to those at the University of Toledo have contributed in different ways to the work over the past year. At Solar Cells Inc, we especially thank Peter Meyers, Teddy Zhou, and R.C. Powell for help and advice in a variety of ways. At NREL, we are grateful for helpful conversations with Bolko von Roedern on many subjects, with Tim Gessert especially on issues relating to sputtering of ZnTe and CdTe, to Richard Ahrenkiel for discussions of PL decay processes, and to Kannan Ramanathan for conversations and the supply of chemical bath coated CdS. At Georgia Tech, Ajeet Rohatgi and Ajit Bhat have been helpful with exchange of samples and other suggestions.

8.0 References

1. A. D. Compaan, R.G. Bohn, A.Aydinli, A. Bhat, C. M. Tabory, L-H. Tsien, S. Liu, M. Shao, M. Savage, and Y. Li, "Thin Film Cadmium Telluride Photovoltaic Cells," Annual Report, Photovoltaic Program, FY 1991. (March 1992). NREL/TP-410-4724. 306pp. (Available NTIS: Order No. DE 92001248.) pp. 167-172.

2. A. Compaan and A. Bhat, "Laser-Driven Physical Vapor Deposition for Thin-Film CdTe Solar Cells," Int'l J. Solar Energy, 20, No. 1-4 (1992).

3. A.D. Compaan, R.G. Bohn, C.N. Tabory, M. Shao, Y. Li, Z. Feng, A. Fischer, and L-H. Tsien, "Thin Film Cadmium Telluride Photovoltaic Cells," Annual Report, Photovoltaic Program, FY 1992. (Available NTIS publication number NREL/TP-410-5335 -- DE93000092.) pp. 162-165.

4. A.D. Compaan, R.G. Bohn, "Thin Film Cadmium Telluride Photovoltaic Cells--Annual Subcontract Report 11/91-10/92." (Available NTIS publication NREL/TP-451-5813, UC category: 273, DE94000201.)

5. A. D. Compaan, C.N. Tabory, M. Shao, Y. Li, A. Fischer, Z. Feng, and R.G. Bohn, "Cadmium Telluride Thin-Film Solar Cells by Pulsed Laser Deposition," Proceedings of the Second International Conference on Laser Ablation (Knoxville, TN April 19-22, 1993) (AIP Conference Proceedings No. 288, 1994) pp. 225-230.

6. A. D. Compaan, C.N. Tabory, Y. Li, Z. Feng, and Andreas Fischer, "CdS/CdTe Solar Cells by RF Sputtering and by Laser Physical Vapor Deposition," Proc. 23rd IEEE Photovoltaic Specialists Conference (Louisville, KY, May 10-14, 1993), pp. 394-399.

7. R.G. Bohn, Y. Li, M. Shao, C.N. Tabory, Z. Feng, A. Fischer, and A. D. Compaan, "Raman, Photoluminescence, and SEM Studies of CdS and CdTe Films Grown by RF Sputtering and Laser Physical Vapor Deposition," Proc. 23rd IEEE Photovoltaic Specialists Conference (Louisville, KY, May 10-14, 1993), pp. 510-515.

8. J. Whitacre, K. McNett, B. Miller, R.G. Bohn, & A.D. Compaan, "NSF Research

Experiences for Undergraduates Summer Projects: 1. Measuring Electrical Properties of Polycrystalline Films, 2. Calibrating a Spectral Quantum Efficiency System, 3. Implementing an Optical Beam Induced Current (OBIC) System," Proc. 23rd IEEE Photovoltaic Specialists Conference (Louisville, KY, May 10-14, 1993) pp. 592-596.

9. A. Compaan, R.G. Bohn, A. Bhat, C. Tabory, M. Shao, Y. Li, M.E. Savage, & L. Tsien, "Thin-Film CdTe Photovoltiac Cells by Laser Deposition & RF Sputtering," Photovoltaics Advanced Research & Development Project (AIP Conf. Proc. #268) ed. by R. Noufi, p. 255 (1993).

10. A.D. Compaan, C.N. Tabory, M. Shao, A. Fischer, Z. Feng, & R.G. Bohn, "RF Sputtering of CdTe and CdS for Thin Film PV," 12th NREL PV Program Review Meeting (Oct. 13-15, 1993), (AIP Conf. Proc. to be published).

11. R. Kubo, Statistical Mechanics, (North Holland, Amsterdam, 1965) p. 153.

12. S. M. Rossnagel, in Handbook of Plasma Processing Technology, Ed. by S.M. Rossnagel, J.J. Cuomo, & W.D. Westwood (Noyes Publications, Park Ridge N.J., 1990) pp. 160-182.

13. M.T. Thomas, in Vacuum Physics and Technology, ed. by G.L. Weissler & R.W. Carlson, (Academic Press, New York, 1979), p. 553.

14. T.A. Gessert, X. Li, T.J. Coutts, A.R. Mason, & R.J. Matson, "Dependence of material properties of rf-magnetron-sputtered, Cu-doped, ZnTe thin films on deposition conditions," J. Vac. Sci. Technol. B (to be published).

15. R.M. Park, M.B. Troffer, C.M. Rouleau, J.M. DePuydt, & M.A. Haase, "p-type ZnSe by nitrogen beam doping during molecular beam epitaxial growth," Appl. Phys. Lett. **57**, 2127 (1990); M.A. Haase, J. Qiu, J.M. DePuydt, & H. Cheng, "Blue-green laser diodes," Appl. Phys. Lett. **59**, 1272 (1991).

16. J. Han, T.S. Stavrinides, M. Kobayashi, R.L. Gunshor, M.M. Hagerott, & A.V. Nurmikko, "Heavy p-doping of ZnTe by molecular beam epitaxy using a nitrogen plasma source," Appl. Phys. Lett. **62**, 840 (1993); I.W. Tao, M. Jurkovic, & W.I. Wang, "Doping of ZnTe by molecular beam epitaxy," Appl. Phys. Lett. **64**, 1848 (1994).

17. S.H. Shin, J. Bajaj, L.A. Moudy, & D.T. Cheung, "Characterization of Te precipitates in CdTe crystals," Appl. Phys. Lett. **43**, 68 (1983); P.M. Amirtharaj & F.H. Pollak, "Raman scattering study of the properties and removal of excess Te on CdTe surfaces," Appl. Phys. Lett, **45**, 789 (1984).

18. Y.S. Tyan, and E.A. Perez-Albuerne, "Efficient Thin-Film CdS/CdTe Solar Cells," Proc. 16th IEEE Photovoltaic Specialists Conference (1982) p. 794.

19. I. Clemminck, M. Burgelman, M. Casteleyn, J. De Poorter, & A. Vervaet, Proc. 22nd. IEEE Photovoltaic Specialists Conf. (1991) p. 1114.

20. M.E. Ozsan & D.R. Johnson, "An Analysis of Interface Structures in CdS/CdTe Solar Cells, "Proc. 12th European PVSEC" (Amsterdam, April, 1994) (to be published).

21. K. Ohata, J. Saraie, & T. Tanaka, Jpn. J. Appl. Phys. **12**, 1641 (1973).

22. D.E. Aspnes, in Handbook on Semiconductors, ed. by T.S. Moss (North-Holland, New York, 1990), Vol. 2, p. 109.

23. R.G. Rodrigues, N.R. Taskar, & J.M. Borrego, "Modulation Spectroscopy Characterization of Solar Cells: CdTe, GaAs, and InP Systems," Proc. 12th European PVSEC (Amsterdam, April, 1994) (to be published).

24. A. Fischer, A. Compaan, A. Dane, & A. Aydinli, "Resonant Raman and Photoluminescence of CdTe Films for PV Using Diode Lasers," in Semiconductor Processing and Characterization with Lasers--Applications in Photovoltiacs, (Stuttgart, Germany, Apr. 18-20, 1994) (to be published).

25. Z.C. Feng, A. Mascarenhas, & W.J. Choyke, "Low Temperature Photoluminescence Spectra of <001> CdTe Films Grown by Molecular Beam Epitaxy at Different Substrate Temperatures," J. Luminesc. **35**, 329-341 (1986).

9.0 Publications

Refereed papers published:

1. A.D. Compaan, R.G. Bohn, "Thin Film Cadmium Telluride Photovoltaic Cells--Annual Subcontract Report 11/91-10/92." (Available NTIS publication NREL/TP-451-5813, UC category: 273, DE94000201.)

2. A. D. Compaan, C.N. Tabory, M. Shao, Y. Li, A. Fischer, Z. Feng, and R.G. Bohn, "Cadmium Telluride Thin-Film Solar Cells by Pulsed Laser Deposition," Proceedings of the Second International Conference on Laser Ablation (Knoxville, TN April 19-22, 1993) (AIP Conference Proceedings No. 288, 1994) pp. 225-230.

3. A. D. Compaan, C.N. Tabory, Y. Li, Z. Feng, and Andreas Fischer, "CdS/CdTe Solar Cells by RF Sputtering and by Laser Physical Vapor Deposition," Proc. 23rd IEEE Photovoltaic Specialists Conference (Louisville, KY, May 10-14, 1993), pp. 394-399.

4. R.G. Bohn, Y. Li, M. Shao, C.N. Tabory, Z. Feng, A. Fischer, and A. D. Compaan, "Raman, Photoluminescence, and SEM Studies of CdS and CdTe Films Grown by RF Sputtering and Laser Physical Vapor Deposition," Proc. 23rd IEEE Photovoltaic Specialists Conference (Louisville, KY, May 10-14, 1993), pp. 510-515.

5. J. Whitacre, K. McNett, B. Miller, R.G. Bohn, & A.D. Compaan, "NSF Research Experiences for Undergraduates Summer Projects: 1. Measuring Electrical Properties of

Polycrystalline Films, 2. Calibrating a Spectral Quantum Efficiency System, 3. Implementing an Optical Beam Induced Current (OBIC) System," Proc. 23rd IEEE Photovoltaic Specialists Conference (Louisville, KY, May 10-14, 1993) pp. 592-596.

6. A. Compaan, R.G. Bohn, A. Bhat, C. Tabory, M. Shao, Y. Li, M.E. Savage, & L. Tsien, "Thin-Film CdTe Photovoltiac Cells by Laser Deposition & RF Sputtering," Photovoltaics Advanced Research & Development Project (AIP Conf. Proc. #268) ed. by R. Noufi, p. 255 (1993).

7. A.D. Compaan, C.N. Tabory, M. Shao, A. Fischer, Z. Feng, & R.G. Bohn, "RF Sputtering of CdTe and CdS for Thin Film PV," 12th NREL PV Program Review (Denver, Oct. 13-15, 1993), (AIP Conf. Proc. No. 306, 1994) pp. 329-334.

Annual Reports published in SERI/NREL Annual Report, Photovoltaic Subcontract Program:

1. A.C. Compaan, R.G. Bohn, A. Aydinli, A. Bhat, L.H. Tsien, S. Liu, Z. Chen, C. Tabory, "Thin Film Cadmium Telluride Photovoltaic Cells and Submodules Fabrication," Annual Report, Photovoltaic Subcontract Program, FY 1990. (NTIS publication SERI/TP-214-4135, UC category 270, DE91002149) pp.137-142.

2. A.D. Compaan, R.G. Bohn, A. Aydinli, A. Bhat, C.N. Tabory, L.H. Tsien, S. Liu, M. Shao, M. Savage, and Y. Li, "Thin Film Cadmium Telluride Photovoltaic Cells," Annual Report, Photovoltaic Subcontract Program, FY 1991. (NTIS publication NREL/TP-410-4724, UC category 270, DE92001248) pp. 167-172.

3. A. D. Compaan, R.G. Bohn, C.N. Tabory, M. Shao, Y. Li, Z. Feng, A. Fischer, and L-H. Tsien, "Thin Film Cadmium Telluride Photovoltaic Cells," Annual Report, Photovoltaic Subcontract Program, FY 1992. (NTIS publication number NREL/TP-410-5335, UC category 270, DE93000092) pp. 162-165.

4. A.D. Compaan, R.G. Bohn, C.N. Tabory, M. Shao, Z. Feng, A. Fischer, and C.Deak, "Thin Film Cadmium Telluride Photovoltaic Cells," Annual Report, Photovoltaic Subcontract Program, FY 1993. (to be published)

Annual Subcontract Reports:

1. A.D. Compaan and R.G. Bohn, "Thin Film CdTe Photovoltaic Cells," Annual Subcontract Report, July 1990--31 Oct. 1991. [Available NTIS #DE92001248]

2. A.D. Compaan and R.G. Bohn, "Thin Film CdTe Photovoltaic Cells," Annual Subcontract Report, 1 Nov 1991--31 Oct 1992. [Available NTIS # NREL/TP-451-5813, DE94000201]

10. Students and Technical Assistants Participating in the Project

Students:

Yuxin Li

M.S. June 1993 — "Photoluminescence Studies of CdS and CdTe Films Grown by LDPVD and RF Sputtering"

Zhirong Feng

M.S. June 1994 — "Photoreflectance and Electroreflectance Studies of CdTe Films and CdTe/CdS Heterostructures"

Ph.D. in progress

Meilun Shao

M.S. August 1992 — "SEM and EDS Studies of CdTe and CdS Films Grown by LDPVD and RF Sputtering"

Ph.D. in progress

Andreas Fischer

Ph.D. in progress

Czaba Deak

M.S. August 1994 — "Electrical and Morphological Properties of Polycrystalline CdS Thin Films"

Technical Assistant:

Charles N. Tabory

REPORT DOCUMENTATION PAGE

Form Approved
OMB NO. 0704-0188

1. AGENCY USE ONLY (Leave blank)	2. REPORT DATE	3. REPORT TYPE AND DATES COVERED
	September 1994	Final Subcontract Report, 1 November 1992 - 1 January 1994

4. TITLE AND SUBTITLE

Thin-Film Cadmium Telluride Photovoltaic Cells

5. FUNDING NUMBERS

C: ZN-1-19019-3

TA: PV431101

6. AUTHOR(S)

A. D. Compaan, R. G. Bohn

7. PERFORMING ORGANIZATION NAME(S) AND ADDRESS(ES)

University of Toledo
Department of Physics and Astronomy
Toledo, Ohio 43606

8. PERFORMING ORGANIZATION REPORT NUMBER

9. SPONSORING/MONITORING AGENCY NAME(S) AND ADDRESS(ES)

National Renewable Energy Laboratory
1617 Cole Blvd.
Golden, CO 80401-3393

10. SPONSORING/MONITORING AGENCY REPORT NUMBER

TP-451-7162

DE94011886

11. SUPPLEMENTARY NOTES

NREL Technical Monitor: B. von Roedern

12a. DISTRIBUTION/AVAILABILITY STATEMENT

12b. DISTRIBUTION CODE

UC-1263

13. ABSTRACT *(Maximum 200 words)*

This report describes work to develop and optimize radio-frequency (rf) sputtering for the deposition of thin films of cadmium telluride (CdTe) and related semiconductors for thin-film solar cells. Pulsed laser physical vapor deposition was also used for exploratory work on these materials, especially where alloying or doping are involved, and for the deposition of cadmium chloride layers. The sputtering work utilized a 2-in diameter planar magnetron sputter gun. The film growth rate by rf sputtering was studied as a function of substrate temperature, gas pressure, and rf power. Complete solar cells were fabricated on tin-oxide-coated soda-lime glass substrates. Currently, work is being done to improve the open-circuit voltage by varying the CdTe-based absorber layer, and to improve the short-circuit current by modifying the CdS window layer.

14. SUBJECT TERMS

thin films ; cadmium telluride ; photovoltaics ; solar cells

15. NUMBER OF PAGES

38

16. PRICE CODE

17. SECURITY CLASSIFICATION OF REPORT	18. SECURITY CLASSIFICATION OF THIS PAGE	19. SECURITY CLASSIFICATION OF ABSTRACT	20. LIMITATION OF ABSTRACT
Unclassified	Unclassified	Unclassified	UL